Chapter 2

Controlled Experiments of Hillslope Coevolution at the Biosphere 2 Landscape Evolution Observatory: Toward Prediction of Coupled Hydrological, Biogeochemical, and Ecological Change

Till H. M. Volkmann, Aditi Sengupta, Luke A. Pangle, Katerina Dontsova, Greg A. Barron-Gafford, Ciaran J. Harman, Guo-Yue Niu, Laura K. Meredith, Nate Abramson, Antonio A. Meira Neto, Yadi Wang, John R. Adams, David D. Breshears, Aaron Bugaj, Jon Chorover, Alejandro Cueva, Stephen B. DeLong, Matej Durcik, Ty P. A. Ferre, Edward A. Hunt, Travis E. Huxman, Minseok Kim, Raina M. Maier, Russell K. Monson, Jon D. Pelletier, Michael Pohlmann, Craig Rasmussen, Joaquin Ruiz, Scott R. Saleska, Marcel G. Schaap, Michael Sibayan, Markus Tuller, Joost L. M. van Haren, Xubin Zeng and Peter A. Troch

Additional information is available at the end of the chapter

http://dx.doi.org/10.5772/intechopen.72325

Abstract

Understanding the process interactions and feedbacks among water, porous geological media, microbes, and vascular plants is crucial for improving predictions of the response of Earth's critical zone to future climatic conditions. However, the integrated coevolution of landscapes under change is notoriously difficult to investigate. Laboratory studies are limited in spatial and temporal scale, while field studies lack observational density and control. To bridge the gap between controlled laboratory and uncontrollable field studies, the University of Arizona built a macrocosm experiment of unprecedented scale: the Landscape Evolution Observatory (LEO). LEO comprises three replicated, heavily instrumented, hillslope-scale model landscapes within the environmentally controlled

Biosphere 2 facility. The model landscapes were designed to initially be simple and purely abiotic, enabling scientists to observe each step in the landscapes' evolution as they undergo physical, chemical, and biological changes over many years. This chapter describes the model systems and associated research facilities and illustrates how LEO allows for tracking of multiscale matter and energy fluxes at a level of detail impossible in field experiments. Initial sensor, sampler, and soil coring data are already providing insights into the tight linkages between water flow, weathering, and microbial community development. These interacting processes are anticipated to drive the model systems to increasingly complex states and will be impacted by the introduction of vascular plants and changes in climatic regimes over the years to come. By intensively monitoring the evolutionary trajectory, integrating data with mathematical models, and fostering community-wide collaborations, we envision that emergent landscape structures and functions can be linked, and significant progress can be made toward predicting the coupled hydro-biogeochemical and ecological responses to global change.

Keywords: critical zone, hillslope, model system, water cycle, carbon cycle, energy balance, soil weathering, geomorphology, plant ecology, microbiology, climate change, coevolution, closure relations, coupled-process modeling

1. Introduction

The structure and function of the critical zone—the interface between the solid Earth and its fluid envelopes—are the product of ongoing coevolution of biota, soils, and landforms. Physical and chemical weathering of the parent material lead to soil formation, landscape denudation, and geomorphic alteration. Biological processes modulate these landscape transformations, as microbial and vascular plant communities establish, compete, and adapt while sequestering important elements, such as carbon and nitrogen, for sustaining life cycles. Gravitational, thermal, and chemical gradients controlling fluxes of water, energy, and nutrients mediate the evolution of the critical zone and are in turn determined by its emergent abiotic and biotic characteristics. The complex linkages between these physicochemical and biological processes and the degree of surface and subsurface heterogeneity they create pose a fundamental challenge to Earth scientists across disciplines attempting to predict changes in critical zone behavior [1–3]. Hydrologists, geologists, biologists, and atmospheric scientists have approached critical zone research primarily from disciplinary perspectives [4], thereby overlooking important spatio-temporal process interactions and feedbacks and introducing inherent uncertainty into parameterizations of resource cycling and ecosystem dynamics. Even when interdisciplinary efforts are made (e.g., [5]), the integrated coevolution of landscapes under change remains extremely difficult to investigate. Field studies generally lack the multifaceted observational density and control needed to capture the wide range and variability of relevant processes. Any natural landscape will also have a history of geologic, climatic, and anthropogenic forcing that cannot be fully known, complicating interpretation of present day "snapshot" observations [2]. Laboratory studies, in turn, offer known boundary conditions and a high level of control but are typically limited in the spatial and temporal scales at which they can be performed. Therefore, effects of multiscale process interactions and heterogeneity on system response cannot be captured, and results may not be immediately transferable to scales relevant for prediction.

http://dx.doi.org/10.5772/intechopen.72325

To bridge the gap between laboratory and field experiments and meet the challenge of understanding and predicting landscape-scale changes in Earth system behavior, the University of Arizona has constructed a new large-scale and community-oriented research facility: the Landscape Evolution Observatory (LEO). LEO consists of three identical artificial landscapes (each with a surface area of 330 m^2) within the environmentally controlled Biosphere 2 facility near Tucson, Arizona, USA. At LEO, experimental manipulation of climate parameters (rainfall, air temperature, relative humidity, and wind speed) is possible at a scale that is infeasible in a typical lab setting, while fluxes of water, solutes, gases, and geological media can be monitored at a detail that is not possible in the field. The threefold replication allows quantifying experimental variability at the landscape level. The primary scientific objectives are to quantify interactions among hydrologic partitioning, geochemical weathering, ecology, microbiology, atmospheric processes, and geomorphic change associated with incipient landscape coevolution. The LEO infrastructure is designed to facilitate investigation of Earth surface processes by rapidly iterating dense experimental measurement with development and validation of coupled computational models.

Scientists working on the LEO project are specifically pursuing an interdisciplinary approach to experimental design by cultivating a collaborative group that includes representation from hydrology, geomorphology, soil geochemistry, atmospheric science, ecology, microbiology, and genomics. Overarching considerations in the design of the landscapes included that (i) interactions between abiotic and biotic process could be effectively studied, (ii) patterns emerging during landscape coevolution across multiple scales could be unambiguously identified, and (iii) results could be linked to ongoing work in natural systems. Eco-hydrological [6, 7], soil erosion, and geochemical [8] modeling were used to aid the design process. The consensual physical model that implements these criteria consists in a zero-order basin shape with convergent topography, an average slope of 10°, and uniform depth and composition of purely abiotic, granular basalt soil with a loamy sand texture. The zero-order basin shape emulates the fundamental geomorphic unit of Earth's uplands, presenting a highly relevant study object that parallels areas under active investigation in the natural environment (e.g., [5, 9]). The convergent topography creates significant spatial variability in slope angle and aspect, thus promoting diversity in net radiation, hydraulic gradients, soil properties, biological community composition, and biogeochemical processes over relatively small land areas. The specific slope angle facilitates transient lateral subsurface flow while largely avoiding overland flow and rapid gully erosion. The minimized initial physical complexity, weatherability, and nutrient-content of these landscapes' soil allow emergent formation of flow pathways, soil spatial heterogeneity, surface morphology, and vegetation patterns to be observed over time.

The experiments performed on these landscapes utilize the control capabilities of the Biosphere 2 facility to generate a variable climate forcing over a period of 10 years. Rainfall sequences are selected to inform specific scientific hypotheses and induce significant spatial and temporal soil moisture variability in a climate that contains wet-dry transitions in both warm and cool seasons. As the initially abiotic landscapes evolve to increasingly complex ecosystems, scientists have the opportunity to address fundamental topics that integrate physical, chemical, and biological processes. These include (i) characterizing the patterns of interdependency between the evolving physicochemical properties of landscapes, the biological

communities that inhabit them, and their water, biogeochemical, and energy cycles, (ii) determining whether simple or complex biological communities, weathering patterns, and flow networks arise as a consequence of differing climate regimes, (iii) understanding how point- to plot-scale processes impact integrated fluxes of mass and energy at the whole-landscape level, (iv) assessing whether knowledge of how and why multiscale heterogeneity in landscape structure forms can enable improved prediction of landscape function under change, and whether existing or new predictive tools are required, and (v) determining whether our present knowledge and observational capacity allow closing the balances of mass and energy at the landscape scale.

The controlled experimentation and dense observations at LEO are combined with mathematical modeling to effectively advance our understanding of landscape evolution and its effects on mass and energy cycling between the landscapes and their overlying atmospheres. Modeling is used to help formalize newly gained process knowledge, infer aspects of the system that are difficult to measure, refine the experimental and instrumental design, and generate cross-disciplinary hypotheses that can be tested in the experiments. Specifically, we are using a "learning cycle" approach in which models are used to predict system response before an experiment is performed, and subsequent targeted experiments are used to improve the models' accuracy. Modeling efforts at LEO focus specifically on (i) integrating existing community model representations of hydro-biogeochemical and ecological processes into a coupled modeling framework and (ii) representing landscape behavior over a wide spectrum of elementary scales, ranging from highly resolved small-scale parameterizations to whole-hillslope integrations. Ultimately, model development provides us with the opportunity to transpose the knowledge gained through the LEO experiment into natural environments and therefore forms a critical basis to improving the accuracy of forecasts of landscape change in the real world.

LEO was fundamentally designed as a community resource to effectively meet targets of scientific merit and broader impact. Acknowledging the complexity of the project and maximizing its use for the Earth sciences and general public, the LEO project seeks to (i) facilitate open and real-time availability of sensor network data, (ii) provide a framework for community collaboration and facility access that includes integration of new or comparative measurement capabilities into existing facility cyber-infrastructure, (iii) foster a community-guided approach to science planning, and (iv) develop novel education and outreach programs. This strategy has already proven successful in informing the landscapes' design and first climate experiments, as well as in informing the public through numerous general media publications, the more than 1000 site visitors per year and hundreds of students trained in Earth sciences.

This book chapter provides a detailed overview of the Landscape Evolution Observatory project. We first present the LEO large-scale controllable research infrastructure, its instrumentation and support facilities, and the integrated modeling framework being developed in feedback with experiments. We then describe LEO's combined capabilities to track important mass and energy balances as well as changes in physicochemical landscape structure and biological communities. This is followed by a discussion of LEO's potential to serve as an experimental platform to study interactions between hydrological, biogeochemical, microbiological, plant-ecological, and geomorphological processes associated with incipient hillslope coevolution. Characterizing those interactions is critical for the advancement of hydrologic and coupled-process models at LEO, which are also discussed. We conclude by summarizing

http://dx.doi.org/10.5772/intechopen.72325

the unique opportunities that this long-term institutional experiment provides for the interdisciplinary Earth science community to make significant progress toward understanding and predicting integrated landscape response to environmental change.

2. The Landscape Evolution Observatory large-scale controllable infrastructure to study coupled Earth-surface processes

2.1. The model landscapes, their atmosphere, and associated infrastructure

The Landscape Evolution Observatory (LEO) is comprised of three model landscapes that were designed and constructed to be exact replicas of each other and to contain landscape features emblematic of upland zero-order basins (hereafter ZOBs). The model ZOBs are contained within steel structures oriented parallel to one another within three adjacent, enclosed bays along the western extent of the University of Arizona—Biosphere 2 facility (**Figure 1**). Individually, the bays include more than 596 m^2 of floor space. The total volume of air that interacts with the landscapes is 12,956 m^3, including 10,712 m^3 within the bays where the model ZOBs are located and 2244 m^3 within the underlying basement where air passes before recirculating to the bay above. The steel structures are generally shaped like rectangular trays, with an average slope of 10° and a southerly aspect. Their interior length and width are 30 m and 11 m, respectively (**Figure 2**). The base of the interior volume of the trays is formed by concrete board, secured to steel slats, and mounted atop structural steel beams. That base is not planar but contains an 18-m long depression that is deepest at the downslope extent of the steel trays and diminishes in depth as it expands upslope. The sidewalls of the trays are all built vertically. The whole interior surface area of the trays was coated with an epoxy primer, which was covered with an elastomeric membrane, then an aggregate-filled urethane coating. At 144 locations along the base of the tray, holes were drilled to allow passage of sensor cables. A length of acrylic tubing

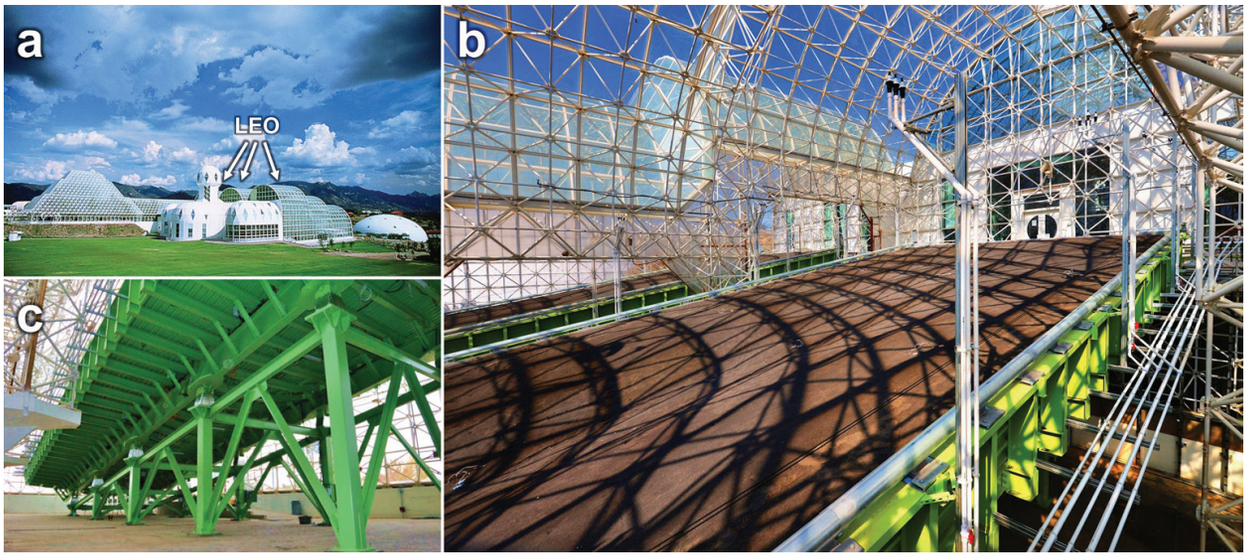

Figure 1. The Landscape Evolution Observatory is housed in adjacent bays within the Biosphere 2 facility (a) and comprises three replicate model landscapes (b) embedded into elaborate steel structures (c).

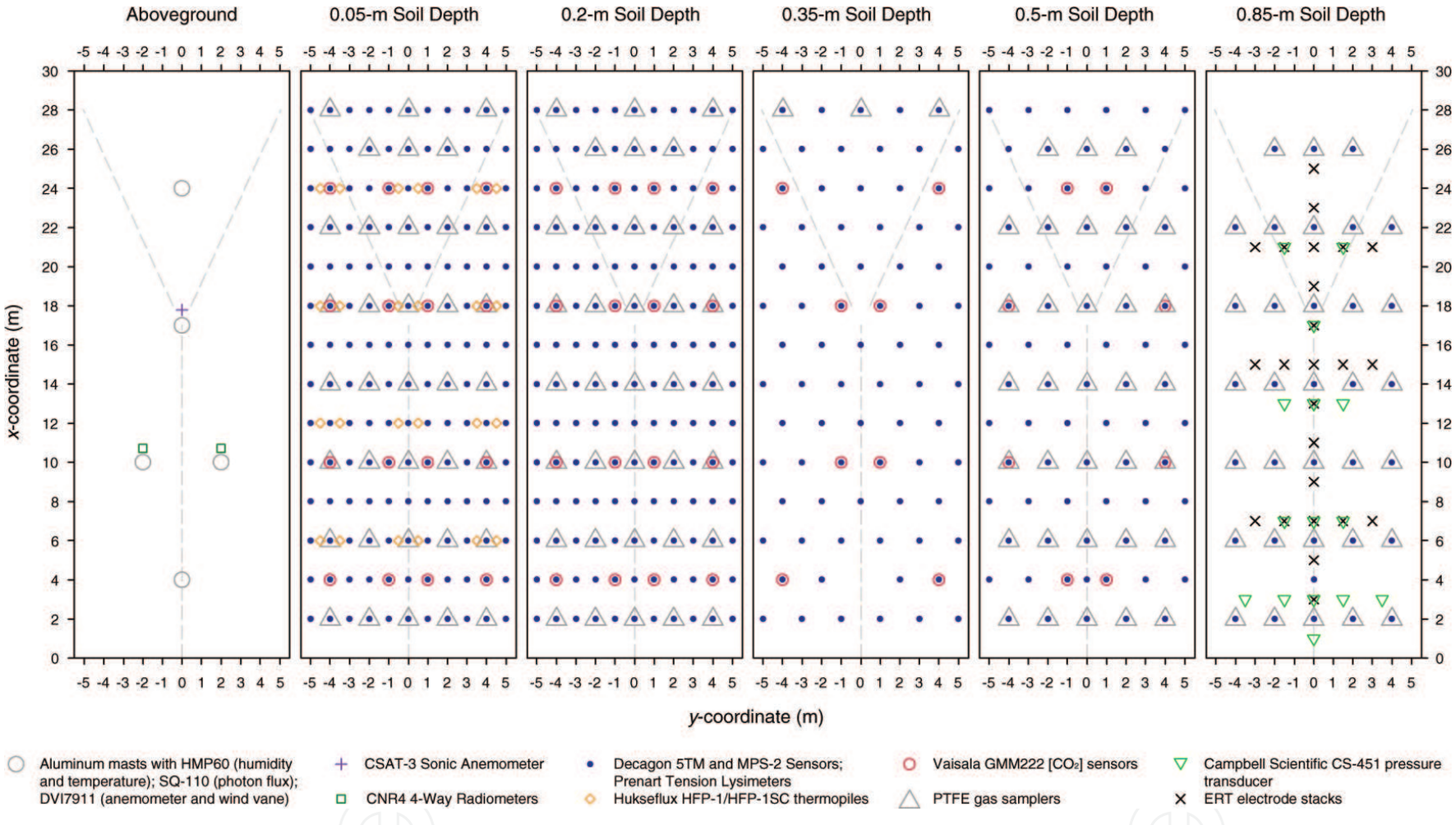

Figure 2. Diagram showing the orientation of the sensor and sampler network in and above the LEO landscapes. The left-most panel shows the approximate lateral (*xy*-coordinate plane) locations of instrumentation aboveground, where sensors are installed at one specific (CSAT-3, CNR4) or five different (all other sensors) heights along vertical aluminum masts. Each of the five remaining panels shows the lateral locations of belowground instrumentation at one specific depth (*z*-coordinate) below the soil surface. Note that CS-451 pressure transducers are actually installed within the structural base of the landscapes at 1-m soil depth, and ERT electrode stacks extend over multiple depths. Dashed gray lines indicate the axes of slope convergence zones.

http://dx.doi.org/10.5772/intechopen.72325

was fitted inside a bulkhead fitting that was sealed into the hole. After final passage of sensor cables through these tubing lengths, they were sealed at their bottom end using expanding foam insulation and epoxy. The base and three of the interior walls of the steel trays are thus impermeable to water. The wall at the downslope extent of the trays was designed to allow water seepage out of the model landscapes. Steel supports and a lattice of steel slats form the primary retention structure of the downslope wall. Porous plastic sheeting was secured to that lattice, which allows water to readily seep out of the landscapes and into six partitioned drainage basins immediately bordering the downslope extent of the landscapes.

The interior volume of the steel structures was filled with crushed basaltic tephra, which comprises the original "parent material" of the model ZOBs. The material was mined from a subterranean deposit of basaltic tephra associated with Merriam Crater in northern Arizona. The mining company was contracted to crush the original rock material down to a loamy-sand texture. The average particle size distribution and elemental composition of the material were reported in [10]. The average sand (50–2000 μm), silt (2–50 μm), and clay (<2 μm) particle-size fractions are 84.6, 12.2, and 3.2%, respectively. The material contains exceptionally low amounts of organic carbon and nitrogen, which was desirable because the target initial condition was a landscape that was effectively abiotic and as spatially homogenous as could be achieved. The loamy sand was hauled from the mining site to LEO and eventually installed within the steel trays by conveyor belt and through manual dispersal and packing by workers. The packing procedure involved incremental installation of four discrete soil layers, each 0.32-m thick when filled into the tray and subsequently compacted to a thickness of 0.25 m. The final bulk density of the packed soil is 1.59 g cm^{-3}, and the porosity is 39% on average. Ground-based laser scans were performed after the installation of each layer, to ensure the greatest possible homogeneity of packing density among individual layers, and across the three replicate model landscapes. The final soil depth on each landscape is, on average, approximately 1 m throughout, though with spatial variability (see Figure 3 in [10]). Because of the designed shape of the underlying steel structure, the ZOBs' surfaces have convergent topography. A primary zone of convergence, or trough, lies near the center of the ZOBs and extends upslope approximately 18 m (**Figure 2**). At that point, the primary zone of convergence terminates at the base of a planar hillslope section that spans to the upslope extend of the ZOBs. Two smaller troughs emanate from this termination point and span toward the upslope corners of the model landscapes. This topographic signature is similar to that observed across many ZOBs in nature [11]. Though the model ZOBs have an average slope of 10°, maximum slopes of approximately 17° exist at that transition from hillslope segments to the primary zone of convergence. The soil should not ever be disturbed by foot traffic or any other source other than natural erosive processes. To accomplish that goal, a personnel transport system was designed and constructed on each landscape (**Figure 3a**). The system allows workers to travel within a railed cart to any point on the soil surface without ever stepping on the surface. This capability is imperative for point-scale measurements of soil and vegetation properties integral to the long-term research agenda.

Irrigation rates of less than 3 mm h^{-1} to approximately 40 mm h^{-1} may be applied individually to each landscape via the engineered irrigation system. In the basement below the landscapes, there are seven storage tanks, each with 8037-liter storage capacity (**Figure 3e**). The tanks are filled with water that is pumped from a local well and passes through a reverse-osmosis

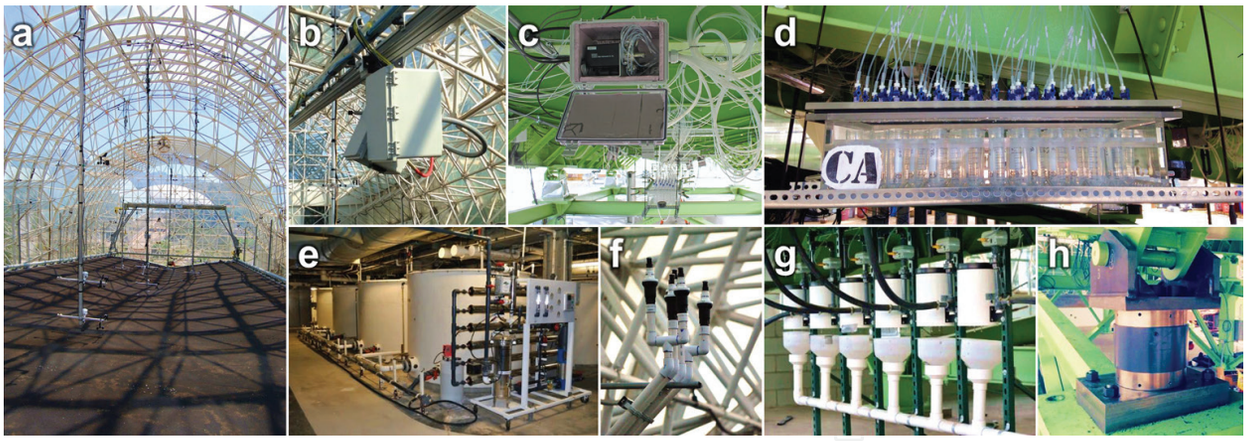

Figure 3. Selected elements of the extensive instrumentation array at LEO: Atmospheric sensors along vertical masts, and personnel transport system in the background (a); high-resolution imaging system mounted to track system (b); multivalves for subsurface gas sampling (c); vacuum box with 55 sample vials for automated collection of soil solution from pore water samplers (d); reverse osmosis system and tanks storing irrigation water (e); sprinkler system for applying irrigation water (f); tipping buckets and flow meters for measuring discharge from six discrete lateral sections of the seepage face (g); 1 of 10 load cells per LEO hillslope measuring changes in total landscape mass.

purification system before storage. The tanks are plumbed such that water can be drawn from any individual tank, or from any combination of tanks, controlled through simple valve selections. Three water pumps deliver water to the landscape level. Here again, the plumbing was installed so that any pump may deliver water to any particular landscape at any time, which provides maximum operational flexibility. At the landscape level, there are five independent plumbing circuits that the water may be delivered to. Each circuit is opened and closed by a programmable valve. Each plumbing circuit dispenses through a unique combination of sprinkler heads (MP Rotator, Hunter Industries, San Marcos, CA, USA) that are located on risers resting approximately 3.3 m above the soil surface (**Figures 1b** and **3f**). There are seven such risers mounted on both the west and east edges of the steel structures containing the model ZOBs. Irrigation water may be dispensed onto the landscapes through any circuit individually or through any combination of the circuits. The spatial homogeneity of applied irrigation varies among the circuits. In general, spatial variability is greatest at low irrigation rates (coefficient of variation, CV > 0.5) and becomes more homogenous at high irrigation rates (CV ≈ 0.2). Disdrometer measurements show that the distribution of water-drop velocities created by the irrigation system approach realistic values of terminal velocity for naturally occurring precipitation. The drop sizes are somewhat smaller than real precipitation [10].

Each bay is enclosed by space frame construction. The exterior of the space frame is covered with 0.011-m thick duo-laminated glass with an interior Mylar sheet. Total solar radiation transmission through the glass is 50–60%, with less than 1% of ultra-violet radiation transmission. The glass is cleaned intermittently. Information about specific transmissions of different wavelengths of radiation was published previously [12, 13]. The space frame directly above the model ZOBs is arranged in three tiers. At the downslope extent, the space frame is approximately 9 m above the soil surface. Across the upper portions of the landscape, the distance to the overlying space frame is greater than 10 m above the surface. At five locations over the landscapes, aluminum masts hang vertically from attachment points on the space frame

(**Figures 2** and **3a**) to an approximate distance of 0.15 m from the soil surface. The masts serve as attachment structures for meteorological instruments that monitor the LEO atmosphere (described in Section 2.1.1). The bottom segment of each mast is telescopic and may be raised to variable heights above the soil surface to accommodate future vegetation growth. A hinged mount connects the masts to the space frame, allowing the masts to be rotated upward to the point of being nearly parallel with the space frame. That action is controlled by motorized winches and braided metal cable that passes through a series of pulleys mounted to the space frame and attaches to the masts at two locations along their length. In this way, the masts can be raised high enough to allow passage of the personnel transport system and to avoid any accumulation and dripping of water during irrigation events, without ever having to remove or rewire any of the meteorological instruments. Air circulation over the landscapes is driven by three air-handler units located in the basement of each bay. These units pull air from a vertical duct that connects the basement and landscape level along the southern extent of the bay. The units push air from south to north through the basement, then vertically through a similar duct on the northern extent of the bay. The air then circulates predominantly from upslope to downslope over the surface of the landscapes. These air handlers are capable of producing maximum air velocities exceeding 1 m s^{-1} over the landscape surfaces—with air velocity being greater near the soil surface and lesser toward the space frame. Additional portable fans can be installed at any time, and at varying locations within the bay, to create greater velocities or turbulence as needed. Coiled radiators within the air-handling units allow circulation of heated or cooled water for temperature and humidity control. These systems are operated through proportional-integral-derivative (PID) controllers, enabling real-time manipulation of air velocities, temperature, and humidity, within some operational constraints. The air space immediately surrounding each landscape is isolated from that in adjacent bays by air partitioning structures consisting of aluminum-pipe framing and twin-wall polycarbonate plastic sheeting mounted to the frame. The air space of each bay is also isolated within the underlying basement by wood-framed walls composed of either plastic sheeting or regular sheetrock.

In addition to the three full-scale model landscapes, a much smaller version of a LEO landscape was built within the central bay of LEO. This scaled-down model, referred to as the miniLEO, was designed as a rectangular cuboid with length of 2 m, width of 0.5 m, uniform soil depth of 1 m, and a 10° slope [14, 15]. Its construction otherwise resembles that of the full-scale models, and it is filled with the same basaltic tephra and equipped with equivalent basic instrumentation, including an irrigation system. The miniLEO is typically used for shorter term experimentation, and destructive soil sampling and complete soil excavations are possible. The primary purpose of the miniLEO is to evaluate measurement and interpretation techniques, optimize experiments (e.g., irrigation sequences), and test specific hypotheses with comparatively low cost and risk before extensive large-scale experiments are launched.

2.1.1. The network of automated, electronic sensors operating at LEO

Here, we outline the array of automated, electronic sensors that are installed in, on, or around the model ZOBs and the measurement capabilities they provide (**Figures 2** and **3**). Other manual sensing and sampling devices utilized within LEO are described in subsequent sections (e.g., an electrical-resistivity tomography system, soil solution, and soil gas sampling). All instruments

described here are connected to a network of Compact Reconfigurable Input-Output devices (CRIOs; National Instruments Corp, Austin, TX, USA), ultimately with data transmission and storage to two onsite servers. Unless otherwise stated, data from each instrument are recorded at 15-min intervals, although this recording interval can be readily adjusted as needed. The instruments and quantities listed below are replicated on each of the three model ZOBs.

Aboveground instrumentation includes:

- *2 Kipp and Zonen CNR4 4-Way Radiometers*—These instruments are mounted at 2-m height above the soil surface on the masts overlying the east- and west-facing hillslope facets adjacent to the central convergence area. Separate radiometers record incoming and outgoing short- and long-wave radiation. The spectral range of measurements provided by the set of radiometers is 300–2800 μm and 4500–42,000 μm. The paired instruments allow comparison of all radiation components on portions of the model ZOBs with different slope aspect.
- *1 Campbell Scientific CSAT-3 Sonic Anemometer*—The instrument is mounted at 2-m height on the mast overhanging the centermost location of the ZOB and oriented upslope. The instrument measures the three-dimensional air-velocity field in high temporal resolution. The instrument is co-located with gas-intake tubing that is routed to an infra-red gas analyzer housed underneath the centermost model ZOB. The sonic anemometer records data at a frequency of 60 Hz.
- *24 Davis Cup Anemometers*—These instruments are located at up to 5 heights along each mast: 0.25, 1, 3, 6, and 10 m above soil surface. No instruments are available at the maximum height at the most downslope mast position, due to the closer proximity of the space frame. They measure wind speed and direction, with an initiation speed of approximately 1.3 m s^{-1}.
- *24 Vaisala HMP60 Temperature and Humidity Sensors*—These instruments are located at the same heights on all masts and measure air temperature and relative humidity within the ranges −40 to 60°C and 0 to 100%, respectively.
- *24 Apogee Instruments Quantum Sensors*—These sensors are also co-located with others on the masts. They measure photon-flux density within wavelengths spanning 410–655 nm.

Instruments installed within the subsurface of the model ZOBs include:

- *24 Huskeflux HPF-1 and HPF-1SC Soil-Heat-Flux Plates*—These instruments are located as 12 pairs, individual sensors within pairs spaced at 1 m, and broader spacing between pairs. They are thermopiles that measure conductive heat transport into the soil profile. They are buried at 0.05-m depth, with an accompanying thermocouple buried at 0.025-m depth, and co-located with soil water content sensors. Actual conductive heat transport into the soil is estimated based on an algorithm provided by the sensor manufacturer, which considers the water content-dependent heat capacity of the soil-water-air mixture.
- *496 Decagon 5TM Soil Water Content and Temperature Sensors*—These sensors measure the dielectric permittivity of wetted soil and convert to volumetric water content using a calibration equation. They also measure temperature with an installed thermistor. A soil-specific

calibration of the sensors was performed by the manufacturer, using the LEO soil, which enables estimates of volumetric water content with accuracy of ±0.025 or better.

- *496 Decagon MPS-2 Soil Water Potential Sensors*—These sensors also measure dielectric permittivity of an attached, wetted ceramic disc that is in equilibrium with soil water. Based on a calibrated relationship between permittivity and water content of the disc, they report soil water pressure across a range from −6 to −500 kPa. The manufacturer-stated accuracy is ±25% of reading.
- *48 Vaisala GMM222 [CO_2] Sensors*—Based on Vaisala's CARBOCAP technology, these sensors are able to measure [CO_2] within air in the soil pore space. They are buried at 48 locations within each model ZOB.

Other instruments installed external to the landscapes include:

- *15 Campbell Scientific CS-451 Vented Pressure Transducers*—These vented pressure transducers record gauge pressure. They are installed within sealed bulkhead fittings with compression caps at 15 locations along the base of the steel structure. The portion of the bulkhead fitting exposed to soil on the interior of the steel structure is screened to allow water intrusion, but not soil. These transducers measure pressure heads of 0 to 2 m and allow monitoring of the spatial dynamics of water table height.
- *10 Honeywell Model 3130 Load Cells*—These loads cells were installed at a nexus point between the primary vertical supports and the lateral beams forming the perimeter of the steel trays. Collectively, the 10 load cells enable accurate and precise measurements of changes in total-landscape mass (due to additions or losses of water). The manufacturer-reported repeatability is 0.05% of full scale.
- *6 SeaMetrics PE102 Flow Meters*—Groundwater seepage from the landscapes flows into one of six partitioned troughs at the downslope extent and then through tubing that leads to these meters. The manufacturer-reported accuracy is 1% relative error across flow rates of 0.11–11.4 liters per minute.
- *6 NovaLynx 26-2501-A Tipping Bucket Gauges*—After passing through the flow meters, the seepage water then flows into one of these tipping bucket gauges. They are calibrated onsite multiple times per year. These provide superior accuracy at very low flow rates compared to the flow meters.

2.1.2. Collection and analysis of soil solution, rainfall, and discharge samples

Sampling of soil solution is facilitated through 496 suction cup pore water samplers (Super Quartz, Prenart Equipment, Frederiksberg, Denmark; pore size <2 μm) that are embedded in each of the LEO hillslopes. The pore water samplers are co-located with the moisture and matric potential sensors (**Figure 2**). Each sampler is connected via a PTFE sampling line to one of 11 custom vacuum sampling modules distributed across the base structure of each hillslope (**Figure 3d**). Each sampling line is equipped with an individual shut-off valve. The modules consist of a Plexiglas vacuum box equipped with a manual pressure regulator, a vacuum gauge,

and a tray capable of holding 55 centrifuge tubes of 50 mL volume for sample collection. Each module is connected to a vacuum manifold. Vacuum is supplied by a total of two single-stage rotary vane vacuum pumps (Model RC0100, Busch LLC, Virginia Beach, VA, USA) located outside of the LEO domain. The vacuum system allows simultaneous sample collection from all 496 samplers on each slope. However, when needed, vacuum application and sampling can be limited to any subset of modules or even any subset of individual samplers. This allows adapting the timing of sampling to in-slope processes, e.g., to the progression of a wetting front. Furthermore, the suction to be used in each module can be adjusted to matric potential recorded by the sensors co-located with solution samplers to ensure that adequate suction is applied to obtain a sufficient sample volume while avoiding excessive draw beyond the immediate vicinity of the samplers. In addition to soil solution sampling, water samples from the seven common irrigation tanks and from two to four custom precipitation collectors per hillslope are collected manually during irrigation events. Finally, custom-built, Arduino-based autosamplers for discrete sample collection at set intervals are in place to collect water samples from the outflow at the base of each hillslope (seepage flow and potentially overland flow) when it is generated.

All collected water samples are archived in freezers at a temperature of –9°C. Biogeochemical sample analysis is performed in an onsite analytical laboratory and can be complemented by isotopic analysis in the isotope and trace gas facility (Section 2.1.3). Prior to analysis samples are centrifuged at 4816 relative centrifugal force for 20 min to remove particulates (Sorvall Legend XTR, Thermo Fisher Scientific Inc., Waltham, MA, USA). The analytical lab is equipped with a Dionex ICS 5000 ion chromatography system (Thermo Fisher Scientific Inc.) with two conductivity detectors for high throughput and concurrent sample analysis for major anions and cations. Further capabilities include solution analysis for dissolved organic and inorganic carbon and total dissolved nitrogen (TOC-L Series total organic carbon and nitrogen analyzer, equipped with TOC-LCSH autosampler; all Shimadzu, Kyoto, Japan), as well as for pH and electrical conductivity (sympHony multimeter, VWR International, Radnor, PA, USA). In addition, selected samples are analyzed offsite for major, trace, and rare earth elements using inductively coupled plasma mass spectrometry (Elan DRC-II, Perkin Elmer, Waltham, MA, USA). Characterization of organic compounds in collected solutions is performed at the Environmental Molecular Sciences Laboratory (Richland, WA, USA) using Fourier transform ion cyclotron resonance mass spectrometry (FTICR-MS).

2.1.3. Stable isotope and trace gas monitoring

Analysis of the concentration and/or stable isotope composition of key molecular species across the hydrologically and biogeochemically relevant landscape compartments (soil, atmosphere, and outflow) of LEO is facilitated by extensive onsite equipment arrays, encompassing state-of-the-art probing interfaces and analyzing instruments. All central equipment is housed in a custom laboratory facility constructed below the central LEO landscape structure. To facilitate stable and gap-free operation of sensitive instrumentation onsite, the laboratory was equipped with uninterrupted power supply, air-conditioning, and zero air (i.e., air that is free of water, CO_2, and contaminants) supply from a lab generator (Aadco Instruments Inc., Cleves, OH, USA), utilizing compressed facility air via a 60-gal in-line back-up reservoir. The facility currently houses four laser-based gas analyzers. The first instrument is an off-axis integrated cavity output spectrometer (OA-ICOS; IWA-35EP, Los Gatos Research Inc., Mountain View, CA. USA) for continuous measurement of the hydrogen (δ^2H–H_2O; $1\sigma < 0.2\%$)

and oxygen ($\delta^{18}O–H_2O$; $1\sigma < 0.05\%$) isotope composition of water vapor [16]. The second instrument is a dual quantum cascade laser absorption spectrometer (QCLAS; TILDAS-D, Aerodyne Research Inc., Billerica, MA, USA) with two tunable lasers to measure continuously and simultaneously the $\delta^2H–H_2O$ ($1\sigma < 0.1\%$) and $\delta^{18}O–H_2O$ ($1\sigma < 0.03\%$) composition of water vapor as well as the carbon ($\delta^{13}C–CO_2$; $1\sigma < 0.03\%$) and oxygen ($\delta^{18}O–CO_2$; $1\sigma < 0.03\%$) isotope composition of CO_2 [17]. The third instrument is a carbonyl sulfide (COS) monitor (mini QCLAS, Aerodyne Research Inc.) for continuous high-sensitivity ($1\sigma < 2$ pptv) trace gas analysis. Finally, a bench-top differential infrared gas analyzer (LI-7000; LI-COR Biosciences, Lincoln, NE, USA) is available for simultaneous high-speed measurements of water vapor and CO_2 concentrations. Details on the respective technologies can be found elsewhere [18–21]. The gas analyzers are interfaced with sophisticated sample conveyance and control systems utilizing custom LabView (National Instruments Corp.) software for automated in-situ monitoring of liquid and gas compositions across the LEO domains.

A multisource liquid sampling system was devised for high-frequency sampling and real-time analysis of seepage water outflow from the three LEO ZOBs utilizing the OA-ICOS instrument. The sampling system uses a four-channel peristaltic pump (Minipuls 3, Gilson Inc., Middleton, WI, USA) to continuously deliver liquid water from a given source to one of four ports of a stainless-steel sampling manifold that is mounted on the tray-holder of an autosampler (LC PAL, CTC Analytics AG, Zwingen, Switzerland) for liquid injection into a vaporization unit and subsequent vapor delivery into the isotope analyzer. This setup delivers robust performance [22] and facilitates water isotopologue analysis of outflow from each LEO landscape at approximately 30-min intervals. To obtain an even higher temporal resolution of discharge isotope composition, as well as for complementary analysis of irrigation, discharge, and soil solution samples, the OA-ICOS instrument and autosampler setup can be used to analyze collected water samples (Section 2.1.2) offline.

Gas sampling is performed in the atmospheres and subsurface soil of each LEO landscape utilizing extensive valving and probing arrays that can be simultaneously linked to the dual-QCLAS, COS, and benchtop gas analyzers. Twenty-four air intake lines, with sheltered inlets at four to five different heights along each of the five masts distributed over each slope surface (Section 2.1; **Figures 2** and **3a**), are available for atmospheric gas sampling. Subsequent sample intake from each of the lines is facilitated by three stream selector valves (VICI Valco Instruments Inc., Houston, TX, USA) situated at the central onsite laboratory, with flow driven by a downstream vacuum pump. To eliminate temporal delay associated with sample gas transport from air inlet to analyzer, the intake line sections upstream of the valves can be constantly purged with fresh atmospheric air using branch-off lines connected to a purge pump via custom vacuum manifolds. To extract air samples from the subsurface, 141 custom soil gas samplers installed in a uniform grid at multiple soil depths are available within each of the model landscapes (**Figure 2**). The samplers were constructed from microporous, hydrophobic PTFE tubing sealed at both ends to gas transport lines with epoxy and heat shrink tubing. A multilevel conveyance system, comprising 27 sub-level stream selector valves mounted at varied locations across the landscapes' structural bases (**Figure 3c**), three main-level selector valves (VICI Valco Instruments Inc.), and several digital mass flow and pressure controllers (Alicat Scientific, Tucson, AZ, USA), allows for automated sampling from the dense probe network according to programmed sequences. The best achievable sample

interval is approximately 1 h for sampling all atmospheric inlets and 36 h for sampling all subsurface probes. Actual sampling frequencies for atmospheric and soil gases vary depending on experimental priorities. All measured trace gas concentrations and isotope abundances in water vapor and CO_2 are calibrated to reference scales using self-built delivery systems for calibration standards (e.g., NOAA and IAEA standards). In addition, and because the isotopic liquid-vapor equilibrium in soils is mainly temperature dependent [23], the measured vapor-phase isotope composition in soil air can be utilized along with measured soil temperatures to infer the liquid soil water isotope composition [24–26] throughout the LEO subsurface.

2.1.4. Remote sensing instrumentation

Each hillslope is equipped with a custom-designed camera imaging system consisting of a hyperspectral imager and a thermal infrared camera. The hyperspectral imager (SOC710VP, Surface Optics Corp, San Diego, CA, USA) produces images within the wavelength range of 400–1000 nm with 4.7-nm bands (128 total bands). The thermal infrared camera (ICI 9640 P-Series, Infrared Cameras Inc., Beaumont, TX, USA) produces images with a 7–14 μm spectral response with a ±1°C accuracy. The images will be used to estimate spatiotemporal patterns of bare soil evaporation, plant transpiration, and photosynthesis (see, e.g., [27]).

In order to image the entire surface of the LEO hillslopes in a precise and repeatable way, the cameras are installed on a 35-m long belt drive linear actuator (MSA-14S, Misumi, Schaumburg, IL, USA), which is suspended from the space frame of Biosphere 2 and hangs 7 m above the surface of the LEO hillslopes at a 10° pitch (**Figure 3b**). This linear actuator allows movement of the camera boxes in the *x*-direction of the hillslopes and provides sub-millimeter linear resolution. A custom robotic stage allows the cameras to pan right and left and provides a 0.2° angular resolution or 1.5 cm at the soil surface. The hyperspectral camera uses a f = 8 mm lens producing an image area of 4.6 × 4.6 m with 0.9-cm resolution at the slope surface, while the infrared camera uses a f = 16 mm lens producing an image of 4.6 × 3.4 m with 0.7-cm resolution. The cameras are housed in an environmentally controlled enclosure to minimize temperature fluctuations using chilled compressed air. The linear actuator and robotic stage allow recording the 27 images required (9 along the *x*-axis and 3 along the *y*-axis) to cover the entire LEO soil surface. The camera system and data offload are controlled using custom LabView software, and software is being developed to stitch the images together to create complete images of the LEO surfaces.

In addition to imaging of the LEO surfaces, a LiDAR scanner (ScanStation C10, Leica Geosystems, Heerbrugg, Switzerland) is used to map surface topography changes in the LEO hillslopes and will be used in the future to measure vegetation growth as plants are introduced. The scanner provides a 6-mm spatial accuracy and 2-mm modeled surface precision. A 6-month scan interval of all hillslopes will provide us with a time series of geomorphologic change.

2.1.5. Electrical resistivity tomography system

Electrical resistivity tomography (ERT) is used for minimal-invasive monitoring of the subsurface at LEO. An ERT survey is performed by injecting an electrical current through a pair of electrodes and measuring the potential at several other electrode pairs. Several current

http://dx.doi.org/10.5772/intechopen.72325

injections are performed at various locations in order to create a set of redundant potential measurements, which are used to derive a set of apparent electrical resistivity values. The apparent electrical resistivity values are then converted to a "true" electrical resistivity set through an inversion procedure [28], which can ultimately be related to soil physical properties (e.g., porosity), water content, and solute concentration [29].

Each LEO landscape is equipped with two current-injecting electrodes and 24 custom potential-measuring electrode stacks (**Figure 4a**). Each electrode stack is installed vertically into the LEO soil and comprises five stainless steel electrodes, separated by insulating acrylic cylinders, for potential measurements at varied soil depths (**Figure 4b**). Each of the 120 total electrodes can be connected to a Supersting R8 (Advanced Geosciences Inc., Austin, TX, USA) electrical resistivity meter and induced polarization and self-potential system. The fully automated eight-channel system allows rapid three-dimensional surveying and sequential imaging of dynamic processes with high accuracy and low noise levels. Specialized software (RES3DINVx64, Geotomo Software, Kardinya, Australia) is used for data processing. The system can provide a spatial resolution of a few centimeters in proximity to the electrodes and is coarser at increased distance from the electrodes.

The Supersting electrical resistivity meter is also used to perform geophysical surveys of the miniLEO small-scale replicate system, where intensive soil sampling is possible to validate ERT measurement and interpretation methods for use on the full-scale LEO landscapes. Specifically, we seek to establish relationships between measured resistivity fields and features of subsurface heterogeneity associated with, e.g., changes in porosity, clay formation, moving wetting fronts,

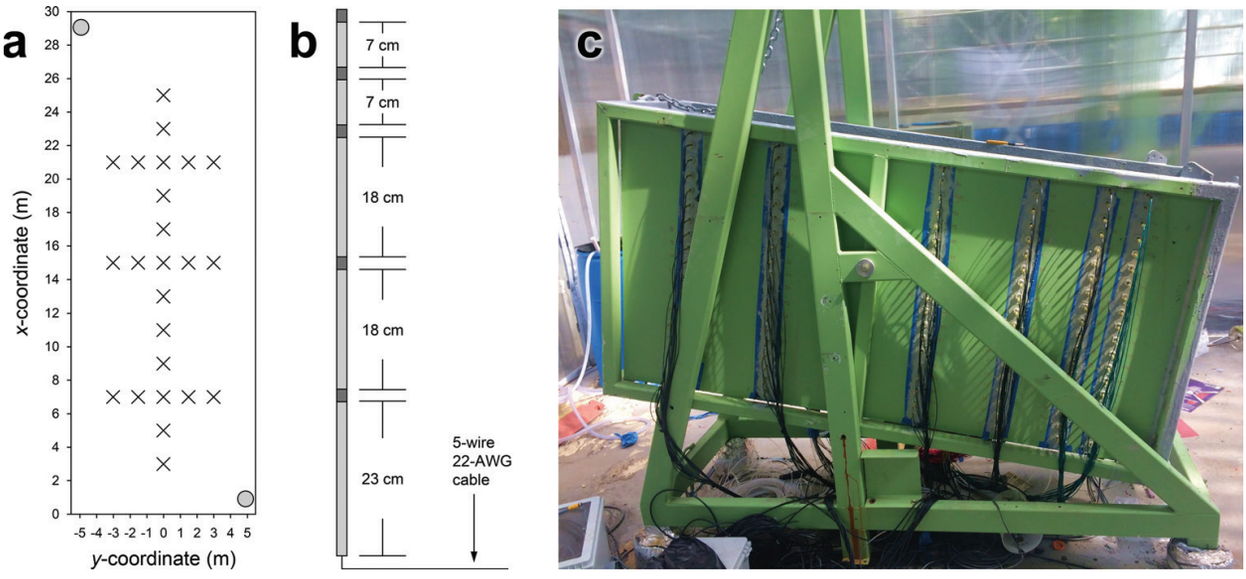

Figure 4. Overview of electrical resistivity tomography (ERT) instrumentation at LEO. (a) Horizontal (*xy*-plane) arrangement of the 2 current-injecting electrodes (gray dots) and the 24 potential-measuring electrode stacks (black x's) across a LEO hillslope. (b) Schematic of an electrode stack, where dark gray sections indicate stainless steel electrodes and light gray sections indicate insulating acrylic rods. (c) The miniLEO small-scale replicate of the LEO hillslopes, equipped with 228 electrodes installed through its walls along 12 vertical transects. This miniLEO setup is used to test and develop ERT surveying and interpretation methods that can ultimately be applied to nondestructively monitor incipient subsurface heterogeneity on the large-scale LEO landscapes.

and plant root distributions. The miniLEO was therefore equipped with 228 electrodes distributed along its walls (**Figure 4c**), allowing for subsurface mapping with particularly high resolution.

2.1.6. Sampling of soil material for physicochemical and biological analysis

Regular soil sampling is required to assess the spatiotemporal microbiological variations and geochemical transformations occurring in the hillslopes. However, soil coring in the landscapes has to be performed conservatively to preserve the topography of the slopes and avoid preferential flow paths following soil removal. Therefore, coring has thus far been limited temporally to a twice-yearly basis (including times before and after irrigation events) and spatially to 4–6 locations corresponding to the zones that are expected to experience divergent evolution (including head slope, convergence zone, toe slope, and side slopes). We use the personnel transport system to access coring locations without disturbing the soil surface. A 1-m long steel corer with 1-inch internal diameter powered by drill and fitted with 1 × 37 3/4-inch plastic liner (AMS Inc., American Falls, ID, USA) is used to collect the samples. For each location, a new clean liner is fitted into the corer to prevent cross-contamination between samples. The plastic sleeve is extracted post-coring and sealed at both ends to prevent soil loss. After core extraction, the resulting hole in the soil is backfilled with the same amount of original tephra material, which is stored in barrels. To ensure that the backfill material is as similar in composition and extent of weathering to the extracted slope material as possible, the barrels receive irrigation water at similar rates as the ZOB soil.

The cores are brought to the lab where their lengths are measured, and they are sub-sectioned according to the depth profile recovered. Each subsection is partitioned into two halves to obtain samples for microbiological and geochemical analyses. Soil sampling areas are co-located with solution samplers and sensors to obtain complementary physicochemical measurements, and modeled variables needed to perform coupled hydro-geochemical and mineralogical analyses.

After extraction, samples for microbiological analyses are either stored on ice or flash-frozen for DNA and RNA extractions, respectively. High-throughput analyses of DNA provide total community composition (amplicon sequencing) and predictions of functional potential (metagenome sequencing), while RNA sequencing (metatranscriptomics) provides expressed function of the community. Soil samples are also used to analyze copy numbers of important functional genes using quantitative real-time polymerase chain reactions (qPCRs).

Samples for geochemical and mineralogical analyses are air-dried, with weight recorded before and after drying to determine moisture content of the sample. Air-dried samples are analyzed to quantify and characterize accumulation of organic compounds and to quantify inorganic carbon accumulation through weathering processes. Content of total nitrogen and total and organic carbon (following treatment with phosphoric acid to remove inorganic carbon) is determined using a total carbon and nitrogen analyzer (TOC-L Series, Shimadzu; see also Section 2.1.2) coupled with a solid sample combustion unit (SSM-5000A, Shimadzu). Molecular characterization of soil organic matter (SOM) to observe carbon stabilization and fractionation during weathering processes is performed using Fourier transform ion cyclotron resonance mass spectrometry (FTICR-MS) at the William R. Wiley Environmental Molecular

http://dx.doi.org/10.5772/intechopen.72325

Sciences Laboratory, a national scientific user facility at the Pacific Northwest National Laboratory (PNNL). Selected soil samples from various depths and along specific flow paths are subjected to solvent exactions (H_2O, MeOH, and $CHCl_3$), and soil extracts are analyzed together with co-located solution samples by FTICR-MS. Air-dried samples are also used for sequential extraction followed by inductively coupled plasma mass spectrometry (ICP-MS) and X-ray diffraction analysis (following size fractionation to concentrate newly formed minerals) to quantify changes in mineralogical composition of the hillslopes. Mossbauer spectroscopy is employed to characterize the oxidation state and bonding environment of iron in weathering basalt in order to trace weathering of Fe-containing phases and precipitation of new minerals.

2.1.7. Integrated mathematical modeling framework

Experiments at LEO are iterated with coupled Earth system modeling. The Terrestrial Integrated Modeling System (TIMS) takes advantage of existing state-of-the-art community models to study interactions and feedbacks between various physical, geochemical, and biological processes by communicating fluxes and states of energy, water, and mass between various component models (**Figure 5**). A model developed in a specific discipline is typically limited by the scope of the developers' expertise and limited knowledge of other disciplines. To compensate

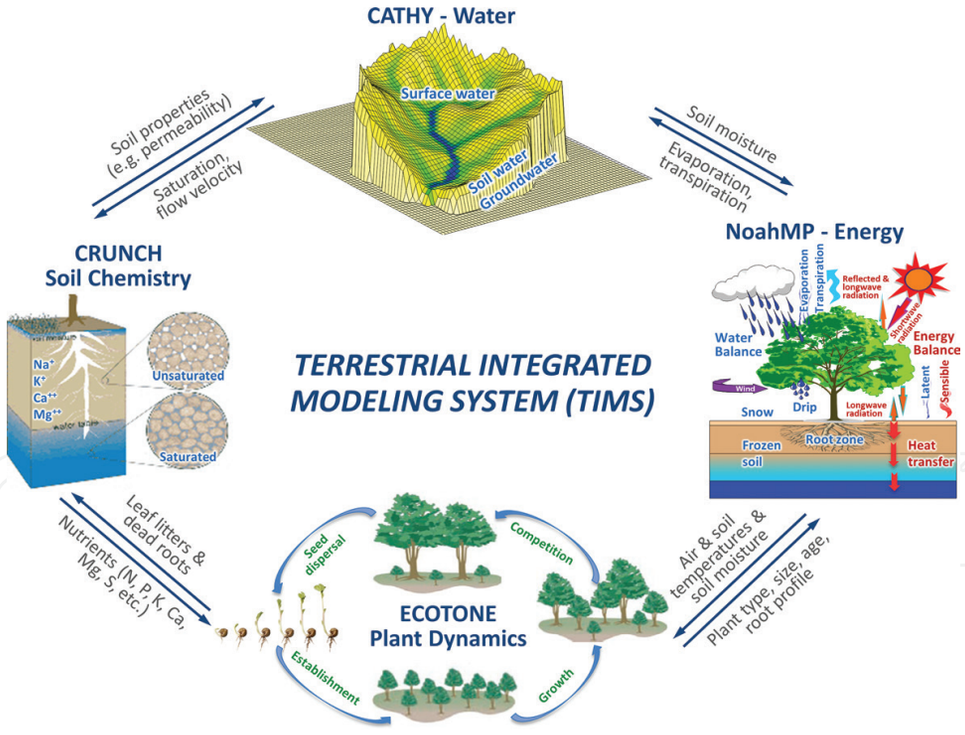

Figure 5. Schematic diagram of the Terrestrial Integrated Modeling System (TIMS) used to inform experiments and formalize observed interactions and feedbacks between physical, geochemical, and biological processes at LEO. TIMS couples existing state-of-the-art community models and aims to simulate the dynamics of (1) surface water in rivers, lakes, and wetlands, subsurface water in the vadose zone and aquifers, (2) organic and inorganic solute transport driven by surface and subsurface flow, volumes of various minerals, and porosity, (3) plant species and biomass distribution over a landscape, and (4) land surface energy, water, and carbon exchanges with the overlying air through atmospheric turbulent transfer and radiation transfer.

for these limitations in the models of individual disciplines, TIMS integrates advanced knowledge and expertise from various disciplines and may thereby exceed the sum of its parts. TIMS has integrated a physically based hydrological model (CATchment Hydrology model, CATHY) and a land-atmosphere energy, water, and carbon exchange scheme (NoahMP) [30, 31]. In addition, it has integrated newly developed modules such as a radiation correction model, which accounts for the effects of topographic shading and scattering [32], and a six-carbon pool microbial enzyme model, which provides the capability to model the responses of soil microbial respiration to soil moisture dynamics [33]. TIMS aims to further integrate an individual-based ecological model (e.g., ECOTONE) and a geochemical model (e.g., CrunchFlow).

CATHY [34] is a 3D, physically based, surface-subsurface coupled flow model. The subsurface flow module in CATHY solves the pressure-based 3D Richards equation describing flow in variably saturated porous media [35], while the quasi-2D surface flow module solves the diffusive wave equation describing surface flow propagation over hillslopes and in stream channels and lakes identified using terrain topography and the hydraulic geometry concept [36]. This model has undergone long-term development and represents one of the most thoroughly developed, physically based flow models. NoahMP [37] represents the land surface energy (e.g., radiation, sensible, and latent heat fluxes), water (e.g., transpiration and evaporation), and carbon fluxes exchanging with the atmosphere and provides multiple physical options for hypothesis testing. It is a community land surface model developed through collaborations among scientists in national centers (e.g., NCAR, NCEP, and NASA) and universities for use in water, weather, and short-term climate predictions (e.g., the National Water Model and the Weather Research and Forecasting Model). It also represents assimilation of carbon through photosynthesis, carbon allocation to various parts of the plant, autotrophic and heterotrophic respiration, leaf litter, root exudates, and dead roots, as well as leaf and root dynamics. ECOTONE [38] is an individual-based ecological model simulating changes in species and associated biomass of individual plants within a patch of land (1–10 m^2 area). Seed germination, establishment of seedlings, and mortality are described by stochastic elements (e.g., seed dispersal, local disturbance), but growth is deterministic based on root distribution and access to water and nitrogen within a competitive context. Resources are distributed to each plant based on the proportion of active roots at each depth relative to total root biomass of all plants. The yearly time step computation is changed to a daily time step to update the biomass in response to daily soil moisture dynamics that are aggregated from CATHY operating at sub-hourly time step. CrunchFlow [39] is a multicomponent reactive transport model describing advective, dispersive, and diffusive transport of solutes, resulting from various chemical reactions such as aqueous complexation, mineral precipitation and dissolution, ion exchange, surface complexation, radioactive decay, and biologically mediated reactions. It also deals with burial, erosion, and compaction of porous media, with an explicit treatment of spatially variable advection of solids as well as reaction-induced porosity and permeability feedbacks to both diffusion and flow.

2.2. Monitoring of hydrologic cycling and flow pathways

Each landscape and its surrounding atmosphere are extensively equipped to close the terrestrial water balance, written as follows:

http://dx.doi.org/10.5772/intechopen.72325

$$\frac{\partial S}{\partial t} = I(t) - Q(t) - ET(t) \quad (1)$$

where S represents the volume of water stored within the landscape (L^3), I represents the irrigation inflow ($L^3\ T^{-1}$), Q represents the discharge outflow at the downslope end of the landscape ($L^3\ T^{-1}$), and ET represents the combined vapor-phase flux associated with bare soil evaporation and plant transpiration from land to atmosphere ($L^3\ T^{-1}$). All variables are functions of time t.

All water balance terms in Eq. 1 can be measured as integrated, landscape-scale states and fluxes at LEO—a capability critical for characterizing hydrologic partitioning under variable environmental conditions yet not achieved in any other experiment at the hillslope scale (**Figure 6a–c**). Temporal changes in water storage within the entire landscape are monitored via 10 load cells installed under the only load-bearing points connecting the main hillslope with the supporting structure. This makes the LEO landscapes the world's largest weighing lysimeters. Volumetric irrigation flow rates are monitored with electromagnetic flow meters. The total specific flux and the spatial distribution associated with each of the five irrigation circuits were characterized through a series of manual calibration trials. The discharge term can comprise both subsurface and overland outflows of water from the landscape, depending on intensity and duration of irrigation forcing. Subsurface flow can exit through one of six lateral subsections of the seepage face at the downslope extent of each landscape and is then routed through

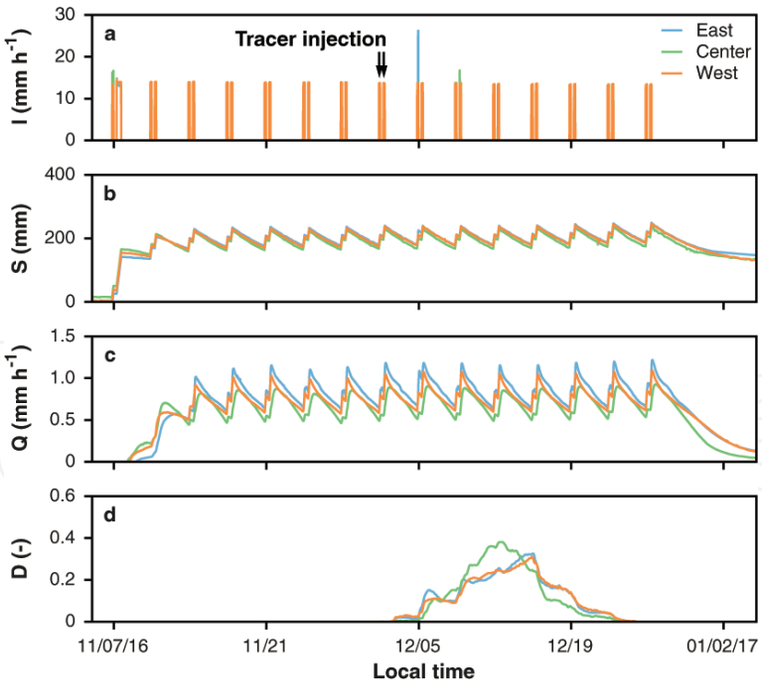

Figure 6. Measured hydrological and tracer dynamics for the three LEO landscapes (East, Center, and West) over the course of a two-month long experiment with periodic forcing and deuterium tracer application during two subsequent irrigation pulses (indicated by black arrows; preliminary data). Data shown are whole-landscape means of irrigation influx (I), water storage (S), discharge (Q), and deuterium tracer abundance in discharge (D; values are relative to the injected deuterium abundance in irrigation water).

a plumbing system with inline electromagnetic flow meters and tipping bucket gauges. Each subsection is measured separately to capture spatial variability of flow, particularly during high flow conditions, and two different types of instruments are used to achieve optimal precision over the full range of possible flow rates. If present, overland flow will be routed over a flume structure and through a plumbing system into an open reservoir, where a pressure transducer continuously monitors changes in water depth. The single remaining water balance component, the combined evapotranspiration flux, can be estimated as the residual term of Eq. 1 using the directly measured rates of all other terms as described above.

The landscape-scale hydrologic cycling is the product of inherently variable surface and subsurface hydrological fluxes and dominantly controlled by landscape heterogeneity [1, 40]. Even in a simplified model system such as the initial LEO landscapes, water movement is not homogeneous [41], and continued coevolution and variable forcing are anticipated to induce increasingly complex flow patterns. The landscape-scale measurements of water storage and fluxes are therefore complemented by spatially resolved measurements utilizing conventional hydrometric as well as innovative, minimal-invasive geophysical and optical techniques. A laterally (154 locations in the *xy*-plane) and vertically (five different depths) dense grid comprising 496 co-located soil water content and matric potential sensors (**Figure 2**) provide meter-scale lateral and sub-meter-scale vertical resolution of water storage, availability, and retention characteristics in continuous time. An even higher spatial resolution of subsurface water dynamics can be achieved using electrical resistivity tomography (ERT) measurements (Section 2.1.5). Three-dimensional time-lapse ERT scans from 24 potential-measuring electrode stacks installed into each hillslope can be geophysically inverted [42] and coupled with hydrological models [43] to resolve decimeter-scale variations in water content and flow processes.

Direct measurements of spatially distributed soil evaporation and plant transpiration fluxes can, in principal, be obtained based on flux-gradient and eddy covariance techniques commonly used in field studies (e.g., [44, 45]). The vapor-phase surface fluxes are mainly determined by wind speeds and a vertical gradient of atmospheric vapor pressure deficit (VPD, a function of air temperature and humidity), and the atmospheric instrumentation array at LEO delivers all required data. Profiles of air temperature, absolute and relative humidity, and wind speed are measured along five vertical masts (at heights of 0.25, 1, 3, 6, and 10 m above the land surface) distributed over each landscape's surface, and high-frequency measurements of the three-dimensional wind vector are available for a central location over each landscape (**Figure 2**). However, application of conventional flux-estimation methods is challenging under the indoor climate conditions at Biosphere 2 [46], as stable atmospheric stratification and associated turbulent intermittency, waves, and other processes make specific methodological adaptations necessary (e.g., [47]). The closed nature of the LEO atmospheres makes it possible, in turn, to use mass balance calculations to approximate whole-landscape evapotranspiration fluxes and their spatial heterogeneity from the spatially stratified measurements. An additional opportunity for measuring spatially resolved evaporation fluxes is through high-resolution thermal imaging. An infrared camera system moving precisely along a track system mounted to the space frame of each LEO bay maps whole-slope soil

http://dx.doi.org/10.5772/intechopen.72325

surface temperature at centimeter-scale resolution (Section 2.1.4). When coupled with atmospheric measurements and known soil properties, the thermal imagery facilitates calculation of surface evaporation using methods similar to those applied by [27]. Given the high density of these spatially resolved aboveground and belowground measurements, good approximations of landscape integrated hydrological states, and fluxes can be attained to corroborate the direct landscape-scale measurements outlined above.

Characterizing the origin, flow pathways, and transit times of water through landscapes is a particular challenge that none of the above instrumentation can meet. LEO was therefore additionally equipped with a state-of-the-art stable isotope facility that operates the first hillslope-scale real-time isotope monitoring network (Section 2.1.3) and performs isotope analysis of collected water samples (Section 2.1.2). Irrigation water can be analyzed and labeled to create a known and time-variable isotope tracer input to the landscapes. Using equilibrium calculations, online measurements from the dense soil gas probing system (141 samplers per hillslope; **Figure 2**) can then be used to track the labeled liquid water through the subsurface soil in continuous time [24]. Isotopic analysis of pore water samples provides additional, spatially detailed (496 samplers per hillslope) snapshots of tracer plumes. Tracer finally leaving the landscapes through evaporation and transpiration can be identified through online gas monitoring along the masts throughout the LEO atmospheres (24 gas inlets per slope), and tracer leaving the landscapes as discharge is recorded using online or offline high-frequency liquid water sampling and isotope analysis (**Figure 6d**). These landscape-integrating and spatially resolved isotope measurements can thus be integrated with mixing models [25], transfer functions [14], and coupled-process models [48, 49] to characterize the pathways and fate of water molecules entering the hillslopes at a given time throughout the LEO domains.

2.3. Monitoring of land-surface energy exchange

The exchange of energy is a key component of the coupling between the landscape surface and the overlying atmospheric boundary layer. The surface energy balance of a LEO landscape can be described as follows:

$$R_{si}(t) + R_{li}(t) + R_{so}(t) + R_{lo}(t) = H(t) + \lambda ET(t) + G(t) \quad (2)$$

where R represents radiative fluxes associated with shortwave and longwave (subscripts s and l) radiation that is incoming or outgoing (subscripts i and o) to or from the landscape (P L^{-2}), H represents the sensible heat flux between land and air (P L^{-2}), λET is the product of the latent heat of vaporization (E M^{-1}) and the magnitude of evapotranspiration (M T^{-1} L^{-2}), and G represents the conductive heat transport and storage into the landscape (P L^{-2}).

The latent heat flux is the only term in Eq. 2 that is measured at the landscape scale. This is accomplished using the known value of heat of vaporization and the whole-landscape evapotranspiration flux estimates, which are based on load cell measurements and mass balance calculations (see Section 2.2). All other terms of the energy balance are measured at several discrete locations across each LEO landscape, and landscape-scale fluxes can be estimated based on the point measurements (**Figure 7c**).

All radiative flux terms on the left-hand side of Eq. 2, and thus the net radiative flux, are measured directly by a pair of four-way net radiometers installed at 1-m height above the soil surface on the two masts located off-axis over the east- and west-facing hillslope segments adjacent to the convergence zone (**Figure 2**). Photosynthetically active radiation (i.e. visible light) is additionally measured at 4–5 heights along all five vertical atmospheric masts. Added uncertainties exist in utilizing these point measurements to represent the average landscape-scale fluxes due to the effects of the windows and structural frames of the climate-controlled bay on solar radiation and mismatched source areas. The conductive heat flux into and out of the ground is measured by 12 pairs of heat flux plates (buried at 0.08 m depth, with associated averaging soil thermocouple probes installed at 0.02 m depth). Those devices are arranged in an approximately uniform grid spanning most of the landscape surface, including monitoring locations below the atmospheric masts (**Figure 2**). Finally, the sensible heat flux from land to atmosphere can be estimated as the residual term of Eq. (2). An alternative possibility for monitoring H, as well as λET, is through application of modified flux-gradient or eddy covariance methods (e.g., [47]). As described in Section 2.2, those methods would utilize the array of aboveground meteorological instruments, but their application under often stable adiabatic conditions above the hillslopes' surfaces poses a challenge and requires methodological developments. Finally, the aboveground and belowground instrumentation allows tracking the spatial and temporal variations in kinetic energy (in terms of temperature, measured at 496 soil locations and 24 atmospheric location; **Figure 7a**, **b**) and latent energy (in terms of humidity, measured at 24 atmospheric location) contained across the LEO domain that result from the local balance of energy fluxes and importantly control hydro-biogeochemical flux and reaction processes.

2.4. Monitoring of biogeochemical cycling

The LEO landscapes are uniquely suited to examine biogeochemical cycling (with the potential to close elemental mass balances) due to the comprehensive array of sensors and samplers installed in and above the hillslopes. In general, a cycle of any element on the landscape can be described in the following common terms:

$$\frac{\partial E}{\partial t} = E_p(t) + E_a(t) - E_r(t) - E_q(t) \tag{3}$$

where E is the element storage in different forms on or within the landscape (M), E_p represents the transfer rate to the landscape with precipitation (M T^{-1}), E_a represents the transfer from the atmosphere through different mechanisms (M T^{-1}), E_r represents the release back into (or new emissions to) the atmosphere (M T^{-1}), and E_q represents the loss with water discharge from the landscape (M T^{-1}). All of these fluxes can be measured, integrated at the landscape scale, and spatially resolved across the landscape using existing instrumentation for major and trace elements. A particular focus lies on carbon, elements essential for plant nutrition, and those indicative of soil formation processes, such as weathering.

Given known rainfall duration and intensity (as well as changes in the mass of the hillslopes), the E_p term can be quantified for the whole landscape by measuring the total element content in rainfall. Measuring element concentrations in the seepage and overland flow (if any) as

http://dx.doi.org/10.5772/intechopen.72325

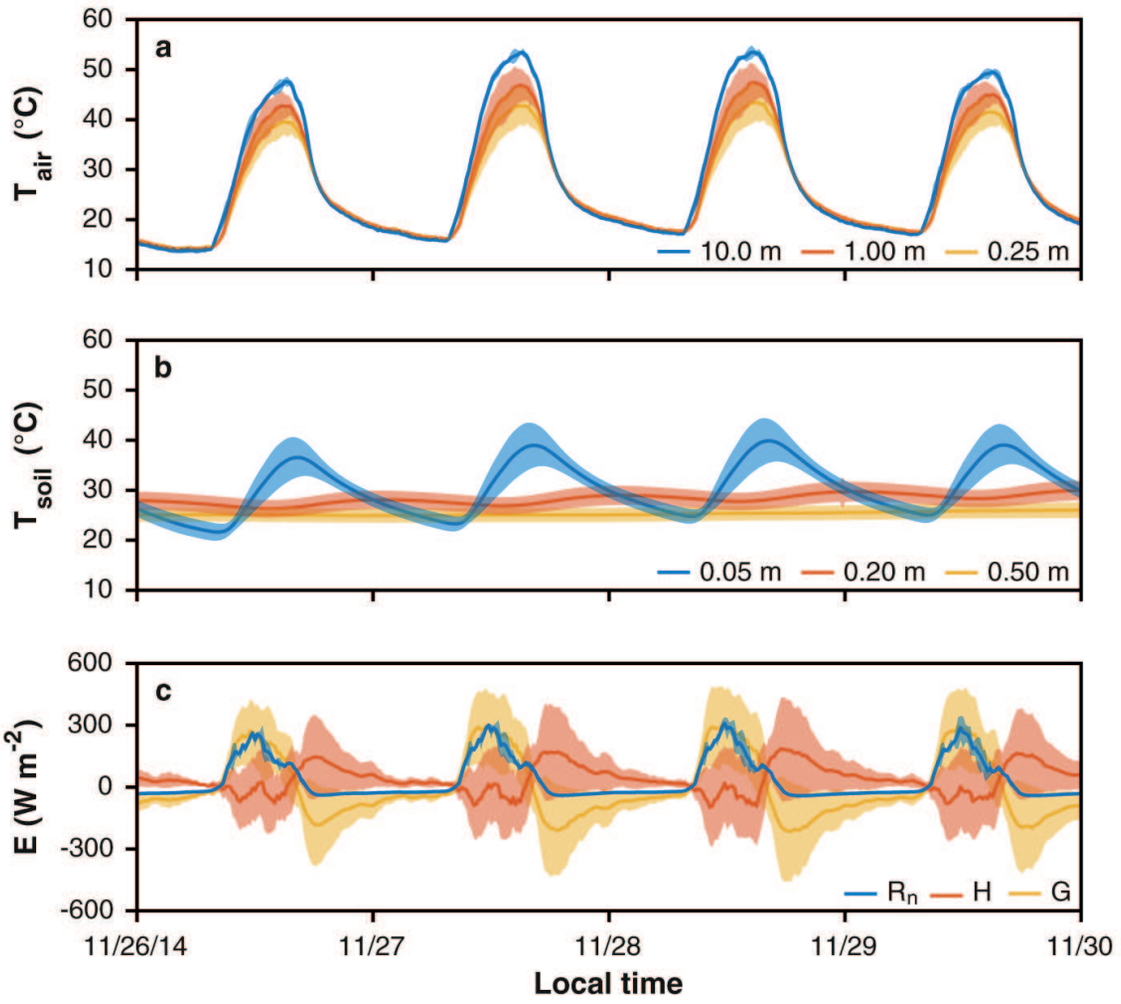

Figure 7. Diel cycles of temperatures and land-surface energy fluxes measured across the domain of one LEO landscape. Air temperatures (T_{air}) are based on all available sensors installed at three selected heights along masts above the land surface, and soil temperatures (T_{soil}) are based on all available sensors installed at three selected depths below the surface. Energy flux (E) observations include the net downward radiative flux (R_n), the upward surface sensible heat flux (H), and the downward ground heat flux into the subsurface medium (G). The latent heat flux was negligible due to extremely dry soil conditions. Solid lines represent whole-landscape means and shaded bounds indicate standard deviations associated with spatial variability across the landscape's domain.

well as seepage volumes per time enables determination of E_q. Autosamplers are installed to capture these water samples during and following all irrigation events on the landscapes. Collected rainfall and seepage samples are analyzed for major cations and anions, as well as total, organic, and inorganic carbon, in addition to pH and electrical conductivity, and a subset is analyzed for major and trace elements (Section 2.1.2).

Exchange with the atmosphere, E_a and E_r, is measured using profiles of gas sampling ports installed above and within the LEO slopes. Atmospheric air can be drawn into the benchtop infrared gas analyzer to measure CO_2 concentrations at approximately hourly intervals (24 samples per slope; see also Section 2.1.3). The gas analysis system is flexible and can also be used for analysis of CO_2 isotope ratios and mole fractions of other gases (such as methane, carbon monoxide, nitrous oxide, hydrogen, carbonyl sulfide, etc.) when connected to alternative

analytical instrumentation such as continuous and discrete gas samplers (e.g., laser spectrometers and gas chromatographs, respectively). The anticipated transfer processes from the atmosphere, E_a, that affect CO_2 dynamics at LEO include ecosystem uptake by photosynthesis, as well as via silicate weathering. Relevant emission processes to the atmosphere, E_r, include a sum of autotrophic and heterotrophic respiration. In systems with well-developed atmospheric turbulence, E_a and E_r are routinely determined from changes in atmospheric concentrations using eddy covariance [50–52] and flux-gradient [45] techniques. However, application of these flux-estimation methods is challenging given frequent temperature and wind speed inversions in the LEO atmospheres, and specific methodological adaptations are required to monitor ecosystem trace gas cycling (see Section 2.2). Currently, with limited expected contributions of biological activity, estimation of the weathering flux of CO_2 can be achieved through in-slope sensors and samplers, as well as through carbonate mass balance of seepage face discharge (see the following paragraph). Microbial respiration is anticipated to increase over time, and once plants are introduced on the landscapes, root respiration, and enhanced microbial activity associated with plant organic matter inputs will increase the biological influence on soil gas concentrations. However, the organic and inorganic carbon export and conserved element export can be used as an estimate of total weathering. The increased complexity of CO_2 net exchange between soil and atmosphere following the introduction of plants will require application and further development of sophisticated flux partitioning approaches to quantify abiotic and biotic components. Currently available approaches focus on partitioning net exchange of CO_2 into the biological gross primary productivity and ecosystem respiration components based on nighttime versus daytime assumptions (e.g., [51]). Nighttime approaches assume that only respiration occurs at night; however, they do not account for CO_2 uptake through weathering reactions. Daytime approaches, in turn, poorly represent daytime respiration and neglect carbonate precipitation. Combining these approaches with use of relationships between CO_2 flux and measured photosynthetically active radiation (PAR) as well as with available measurements of trace gases homologous to CO_2, such as COS [53] and CO_2 isotopologues [50, 52], can help constrain the spatial and temporal mechanics of CO_2 flux processes at LEO and improve empirical and process-based models.

Changes in landscape storage of the elements obtained using estimates of influxes and outfluxes of the hillslopes can be verified by direct measurements of the storage in the landscapes through time. This is made possible by analyzing element concentrations in (i) the solution phase collected from 496 suction lysimeters distributed across each hillslope, (ii) the gas phase obtained using 141 soil gas samplers and 48 Vaisala [CO_2] sensors, and (iii) the solid phase extracted by coring of the soil for subsequent analysis. Solution and gas sampling are nondestructive, and the main limitations on frequency and density of sampling are cost and time of the analyses. Soil coring, in turn, is destructive and has to be used conservatively in order to avoid impacting hillslope behavior (see Section 2.1.6). The unique ability to close elemental mass balances was demonstrated for carbon by [54]. The study was conducted early in the LEO project, when no vegetation was present and most of the carbon fluxes were assumed to be controlled by abiotic processes, driven by weathering of basalt substrate. We quantified atmospheric CO_2 consumption by basalt weathering using pore gas concentration data (from Vaisala sensors) and carbon input with rainfall and export with seepage by analysis of rainfall and seepage solutions for inorganic carbon. Storage of total inorganic carbon (TIC) in

http://dx.doi.org/10.5772/intechopen.72325

the solution phase was quantified as the product of TIC concentrations obtained via the pore water samplers over time and the moisture contents measured by co-located sensors. The study demonstrated that the estimated change in storage was consistent with the difference between incoming and outgoing carbon fluxes (**Figure 8**), validating the capacity of the LEO system to close the carbon mass balance. Employing various densities of pore water sampler data for these calculations further showed that a decrease in data density by one order of magnitude (from about 350 to 35 samples per hillslope) does not significantly affect solution storage estimates for carbon at LEO.

For lithogenic elements, such as Si, Na, Ca, K, Al, and Fe, inputs and outputs to and from the atmosphere are negligible (dust deposition is minimized by the superstructure), but their mass balance is strongly impacted by weathering processes that release a fraction of these elements from rock into solutions that are exported as seepage water (i.e., "from land to rivers"). A fraction of the element mass released from rock by weathering is retained within the landscape in secondary mineral form, promoting the formation of reactive soil interfaces and transforming the pore size distribution with important feedbacks to hydrologic flows. Measuring concentrations of these elements in seepage waters enables a quantification of terrestrial-to-aquatic effluxes [54], while in-slope measurements from pore water samplers

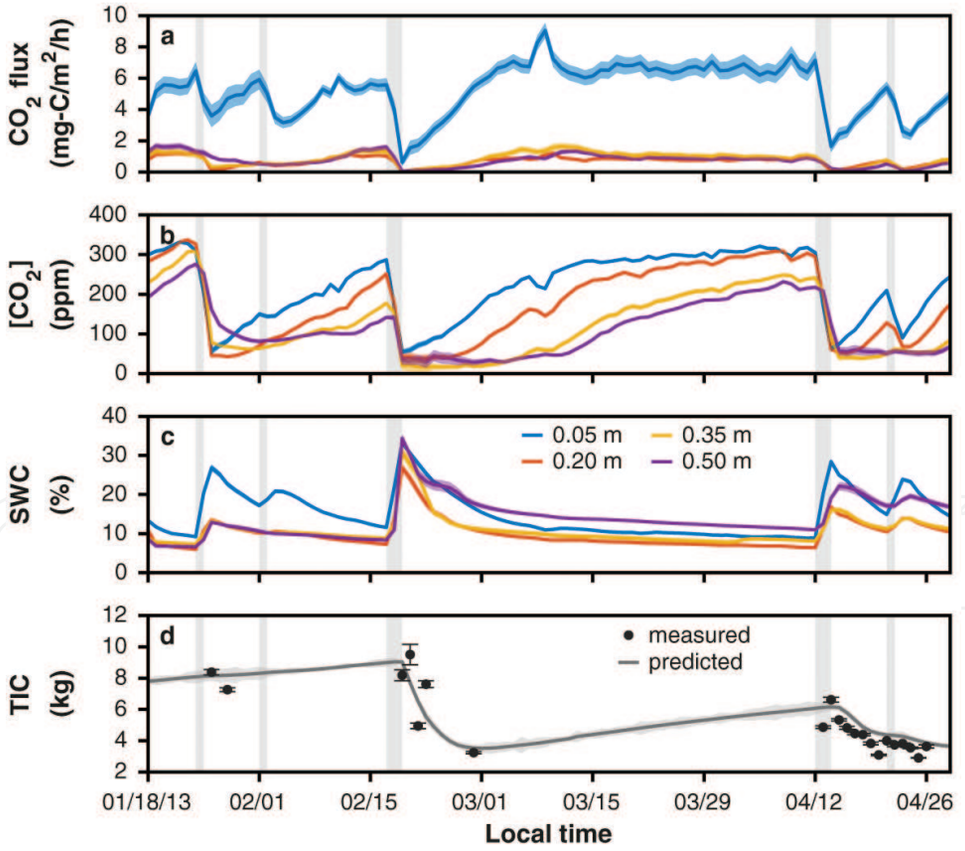

Figure 8. Time series of calculated CO_2 fluxes (a; positive values indicate fluxes from the atmosphere into the soil), gas-phase CO_2 concentrations (b), soil water content (SWC; c), and total inorganic carbon storage (TIC; d) of a LEO landscape over several rainfall events (indicated by gray vertical bars). TIC storage was predicted using incoming and outgoing fluxes (solid line) as well as integrated from measured concentrations in pore solutions (dot markers). Shaded bounds and error bars indicate 95% confidence intervals associated with each variable.

enable characterization of the spatial and temporal variability in the trajectory of mineral transformations and soil formation [55].

2.5. Monitoring of biological community composition and function

Microbial community dynamics on LEO are monitored via soil core collection (Section 2.1.6) to identify pioneering microbial species and metabolisms and to describe the response of microbial communities to environmental forcing (e.g., rainfall) and their longer term successional patterns. This approach provides information on the long-term reciprocal impact of landscape evolution on microbial community composition and function. High-throughput amplicon sequencing of 16S rRNA genes to target the bacterial and archaeal communities revealed significant differences in relative abundances for samples collected from the LEO landscapes before and after rainfall (**Figure 9**) with distinct depth-dependent community distribution profiles of the soils (**Figure 10**). We expected microbes to be distributed nonrandomly along environmental gradients in accordance to their metabolic strategies as observed in the scaled-down mini-LEO model (**Figure 11**; [56]). The phylogenetic distribution observed in the cores extracted from LEO soils was significantly different from that of the parent material [56] and revealed heterogeneous microbial community establishment and development in an otherwise nearly homogeneous soil system. Furthermore, significant differences in pre- and post-rainfall community structure suggest a dynamic system that responds to rainfall events, which may have implications for accelerating bio-weathering rates. Additional genomic and transcriptomic sequencing efforts will reveal functional diversity (gene abundance) and gene-expression profiles, respectively, in the hillslopes. An integrated understanding of microbial community diversity, gene abundance, and functional potential alongside geochemical changes, CO_2 fluxes, and hydrological flow paths can potentially reveal predictive patterns of landscape evolution.

Plant community function, composition, and organization will be monitored through a blend of direct and remote-sensing approaches. Using the personnel transport system that operates over the LEO structure, we will measure leaf-level carbon and water exchange to inform our mass balance equations and to examine interspecific variation in plant function, as it is extensively done outside model systems in critical zone research [57, 58]. Coupling these point-specific measures with multispectral and thermal imaging (Section 2.1.4) will provide spatial patterns of function across the artificial landscape, and the repeated image acquisition through time will provide insights into temporal dynamics. Hyperspectral analysis of ecosystems can yield remarkable insights into vegetation function, and "signatures" of spectra specific to plant species can also be used for mapping distribution across the landscape. The use of narrow (<5 nm) band spectrometers allows for the observation of many ecological features such as pigment composition and content, canopy water content, dry plant litter and wood, and foliar chemistry (e.g., [59] and references therein). Photosynthesis, or gross primary production (GPP), is the largest global land surface carbon flux [60, 61], but the spatially explicit approaches to quantify GPP based on meteorology-driven land surface carbon cycle models, MODIS-based remote sensing, and typical eddy flux tower measurement driven models carry large uncertainties [62, 63]. GPP is directly correlated with solar-induced chlorophyll fluorescence (ChF), because both are driven by absorbed radiation [64–67]. This correlation

http://dx.doi.org/10.5772/intechopen.72325

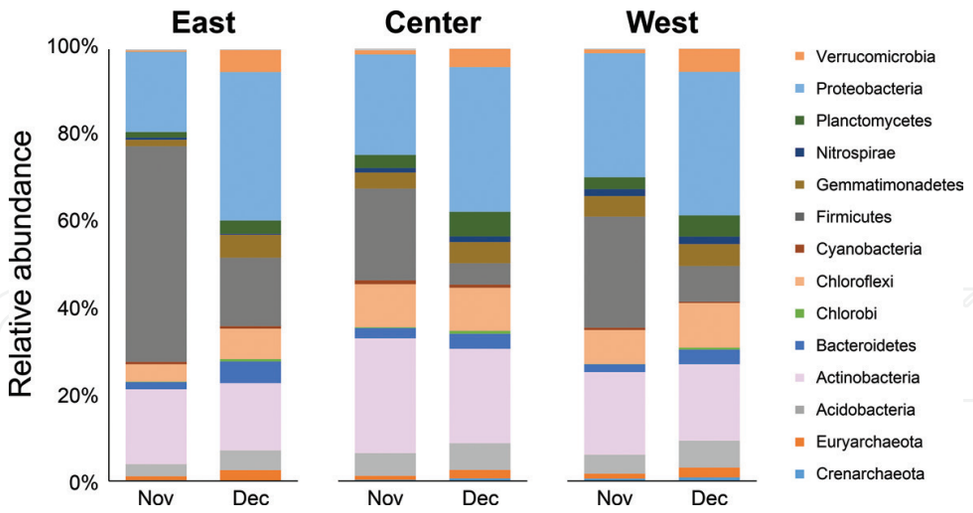

Figure 9. Relative abundance of the 14 most abundant bacterial and archaeal phyla in the three LEO landscapes (East, Center, and West) before (November) and after (December) a series of irrigation events (preliminary data).

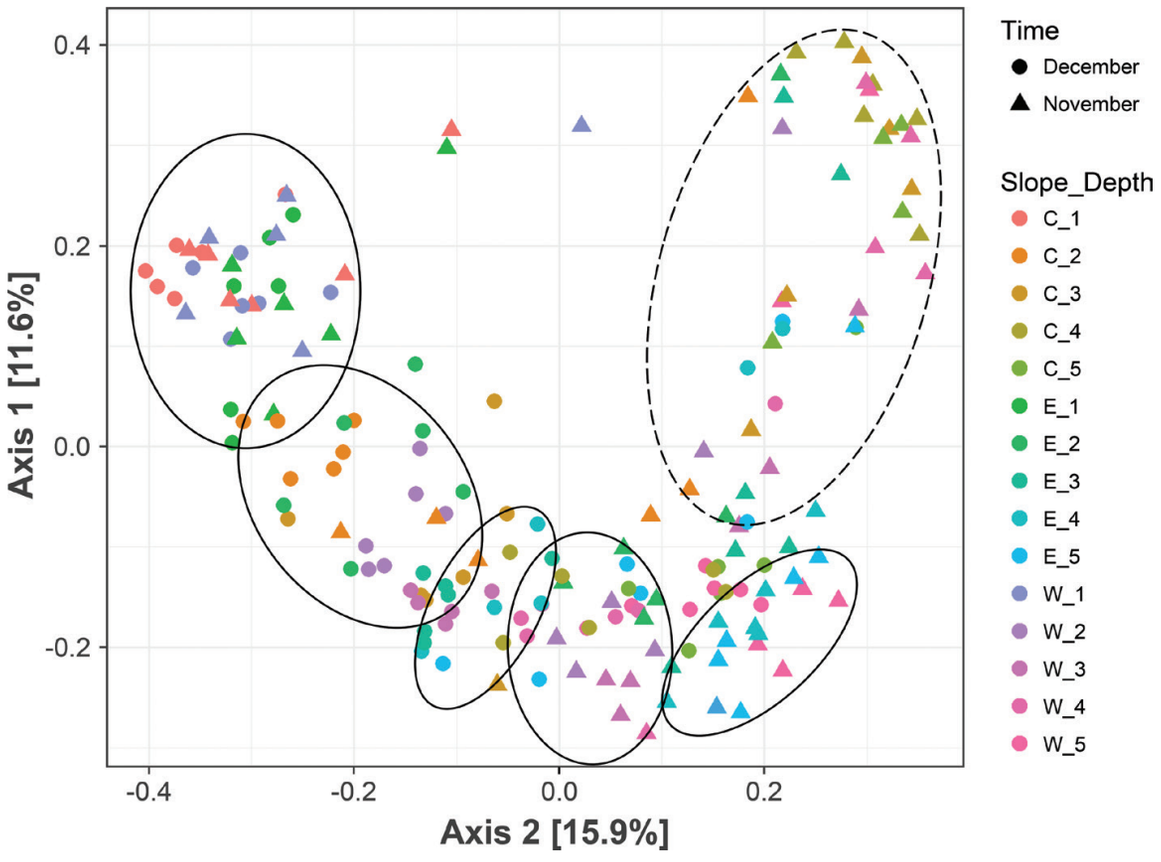

Figure 10. Bray-Curtis ordination of microbial community composition in the East (E), Center (C), and West (W) landscapes before (November) and after (December) a series of irrigation events (preliminary data). Soil depths are indicated by integers representing increments of 15 cm and starting at the surface (number 1). Depth-dependent clustering is observed for December samples and most November samples (solid-line ellipses), while November samples from intermediate depths reveal a more widely distributed pattern (dashed-line ellipse).

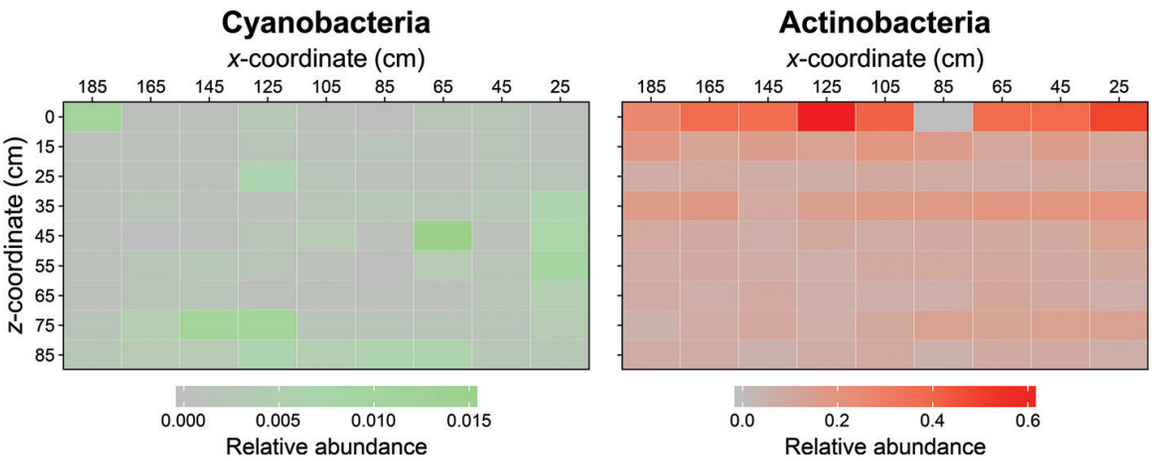

Figure 11. Relative abundance of two major phyla (*Cyanobacteria* and *Actinobacteria*) across the lateral (*x*-coordinate; long axis) and vertical (*z*-coordinate) dimensions of the miniLEO small-scale replicate model. Rectangles indicate unique voxels of volume 200 cm^3 (increments of 20 cm in the lateral and 10 cm in the vertical direction). Samples were collected from each voxel, followed by DNA extraction and high-throughput sequence analysis.

is the result of a reduction in ChF and photosynthesis yield following increases in heat dissipation under high light conditions. Chlorophyll fluorescence is the re-emission of absorbed photosynthetically active radiation (400–700 nm) by the plants at higher wavelengths in the visible red and near infrared (660–800 nm). We will use spectral features around the higher wavelength because the lower band is affected by the re-absorption of chlorophyll pigments, while the higher one is minimally affected by chlorophyll re-absorption effects [68].

2.6. Monitoring of subsurface structural development and pedogenesis

The dense sensor and sampler arrays at LEO offer the capabilities (i) to characterize in great detail the spatial and temporal variability of solution chemistry for a small ZOB (via solution sampling and analysis; see Sections 2.1.2 and 2.4) and (ii) to monitor in high resolution the subsurface structural development (via electrical resistivity tomography surveys and soil coring; see Sections 2.1.5 and 2.1.6) critical during incipient stages of landscape evolution. Together, these capabilities enable the establishment of cause-and-effect relations in soil formation. Known inputs of rainwater, which act as both solvent and transport vector, drive the dissolution of primary mineral surfaces and increase in pore water saturation with respect to secondary mineral phases, including carbonates. Precipitating solids can passivate the surfaces of primary minerals against further dissolution [69]. They also contribute to stabilization of organic carbon against leaching, to mineralization by interacting with newly formed minerals [70–72], and to soil retention of plant-available water and surface-exchangeable nutrients in plant-available form.

Dissolution of primary minerals and precipitation of clay-sized secondary minerals lead to shifts in particle size distribution of the soils toward finer materials. This is predicted to be correlated to flow patterns across the landscapes [8]. In addition, precipitation of poorly crystalline silicates, phyllosilicate clays, and sesquioxides as well as additions of carbon, initially from microbial activity and later from plant root exudation, promote aggregation of the primary particles resulting in changes of the hillslopes' physical structure. The application

http://dx.doi.org/10.5772/intechopen.72325

of electrical resistivity tomography (ERT) provides an opportunity to observe nondestructively the subsurface structure changes of the initially homogenous crushed basalt tephra in response to hydrological (e.g., surface-subsurface water interactions) and biogeochemical processes. Through geophysical inversion of the three-dimensional resistivity field recorded by the ERT system, changes in soil physicochemical properties (e.g., pore volume) can be mapped at high spatial resolution. The combined above observations, especially within the saturated zone, can resolve the spatial distribution of biogeochemical transformations due to abiotic and biotic processes in a pedogenic environment.

Pore water geochemistry can be used to predict the initial stages of basalt weathering, while soil coring samples can validate predictions based on pore water geochemistry. The coupling of pore water data and soil coring data enables measurements of elemental partitioning during the basalt weathering. Therefore, the cycle of a given element on the landscape can also be described by rewriting Eq. 3 as follows:

$$\frac{\partial E}{\partial t} = \frac{\partial E_{aq}}{\partial t} + \frac{\partial E_{s}}{\partial t} + \frac{\partial E_{g}}{\partial t} \tag{4}$$

where subscript *aq* represents the aqueous phase (where concentrations *E* can be measured from pore water samplers), subscript *s* represents the solid phase (where concentrations *E* are derived from soil coring), and subscript *g* represents the gas phase (where concentrations *E* can be obtained from gas sensors and samplers). The gas-phase term only applies when quantifying the partitioning of elements that form gaseous compounds, such as most importantly carbon.

Figure 12 demonstrates the onset of carbon and nitrogen accumulation on the LEO hillslopes as measured from soil cores. While organic carbon and total nitrogen accumulations are mostly limited to the soil surface, inorganic carbon tends to precipitate in a lens in the center of the hillslope. This supports observations of developing heterogeneity in calcite saturation indices on the slopes [55]. Collected soil samples are also analyzed by synchrotron-based (for higher sensitivity) X-ray diffraction to examine changes in mineral composition of the soil, particularly formation of secondary crystalline minerals. By further examining the change of element availability in the solid phase by sequential extraction, it is possible to characterize operationally the formation of X-ray amorphous phases and to better understand geochemical transformations in the soil. In addition to bulk measurements, stabilization of organic carbon in the soils—an integral part of soil formation and important mechanism of carbon sequestration from the atmosphere—is being examined for selected soil samples by Mossbauer spectroscopy, high-resolution transmission electron microscopy (HRTEM), scanning electron microscopy (SEM), high spatial resolution secondary ion mass spectrometry (NanoSIMS) analysis, and X-ray photoelectron spectroscopy (XPS). Release and fractionation of dissolved organic matter are also being examined using Fourier transform ion cyclotron resonance mass spectrometry (FTICR-MS) analysis of pore waters and soil sample extracts. The microbiological analysis of the soil cores (Sections 2.1.6 and 2.5) can address variations in carbon cycling and nutrient availability in addition to linking biological and abiotic processes during the initial stages of basalt weathering and pedogenesis.

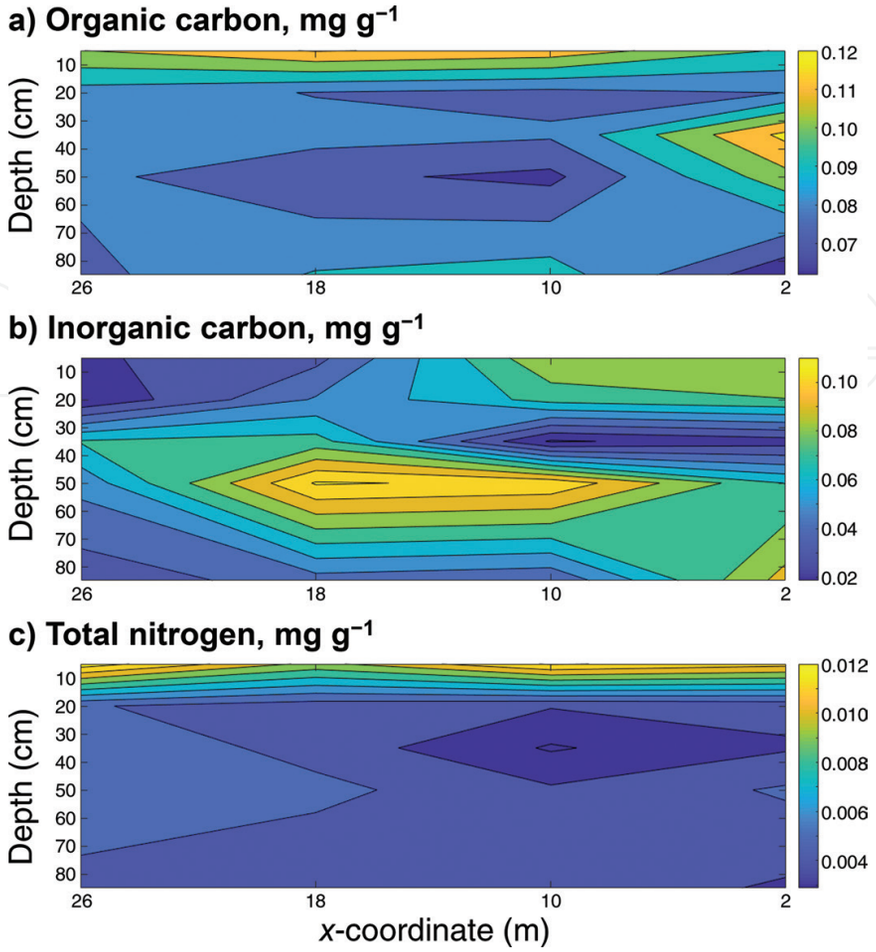

Figure 12. Distribution of organic carbon (a), inorganic carbon (b), and total nitrogen (c) over a cross section of a LEO hillslope 3 years after inception (preliminary data). The cross section spans the depth (*z*-coordinate) and length (*x*-coordinate) of the hillslope through its central plane (i.e., *y*-coordinate equal to zero).

3. Research on integrated hillslope coevolution to improve predictions of landscape-scale change

The LEO landscapes and their extensive instrumentation and control capabilities allow us to track every step along the evolutionary trajectory of a ZOB-scale system, from purely abiotic substrate to living, breathing ecosystems. Emulating their real-world archetypes, the convergent topography of these landscapes promotes spatially variable substrate and resource availability, which is anticipated to eventually facilitate biological diversity and influence how the landscapes filter precipitation and sequester carbon from the atmosphere. Refining our understanding of and our ability to predict how these and other significant ecosystem services are affected by landscape evolution, climatic variability, and long-term environmental change is the central goal of Earth scientists working in the LEO project. This section discusses current foci of research at LEO that target this goal by advancing understanding of how hydrological and geochemical (Section 3.2), microbiological (Section 3.3), and plant-ecological (Section 3.4) processes interact to drive the coevolution of incipient hillslopes and their mass and energy cycling. Concepts underlying

these research foci and early results from initial experiments are presented. The process research at LEO is complemented by the development of hillslope-integrated parametrizations and distributed coupled-process modeling approaches that are hoped to ultimately allow improved prediction of real-world systems' behavior in a changing environment. These modeling approaches are described first (Section 3.1) and with emphasis on hydrologic predictions.

3.1. Changing paradigms for hydrologic prediction at the hillslope scale

In recent years, there has been a paradigm shift in our understanding of flow and transport at watershed scales and in our approaches to prediction. The complexity and heterogeneity of water movement within individual landscape units have been recognized in hillslopes [73, 74], riparian areas [75, 76], and within streams and their hyporheic zone [77]. This has led to calls for new predictive approaches that go beyond the traditional continuum models (i.e., Richards and Saint-Venant equations for flow and convection-dispersion/diffusion equations for transport) [40, 78–80], as these generally rely on calibrated "effective" property values to replace the spatially distributed properties of the landscape—those are essentially unknowable at catchment scales using current technology.

New approaches have sought ways to represent flow and transport directly at the scales of interest, with the expectation that the new equations may differ in form, not just in the parameters [79], from the continuum-scale equations. The concept of a representative elementary watershed, or REW [78, 81–83], provides a framework for representing flow through individual landscape elements and in a river network based on a rigorous time-space averaging of the conservation laws for mass, energy, momentum, and entropy. However, these equations are not complete. They require specification of "closure relations" that specify the boundary fluxes exchanged between these landscape elements in terms of their states and are parameterized by measurable properties of the landscape. These closure relations must represent the aggregate effect of the unresolved sub-REW heterogeneities and flow complexity without resolving them explicitly, and they have been termed the "Holy Grail" of scientific hydrology [78].

An overarching objective of the LEO project is to develop closure relations for hillslope-scale hydrologic flux and transport [7]. These closure relations are parameterizations of the fluxes that cross boundaries between hydrologically relevant units of the landscape [78, 81]—an elementary example is a storage-discharge relation [84, 85]. Taken broadly, such parameterizations are a component of all hydrologic models, but LEO is a useful experimental tool for developing closure relations at the scale of hillslopes [7]. At LEO, it is possible to observe boundary fluxes—and how they emerge from the distribution of internal state variables—with a precision not possible in real landscapes and at a scale not possible in bench-top experiments. Through experimentation and iterative modeling using both lumped and highly resolved models, efforts at LEO are driving toward a suite of hillslope closure relationships that (ideally) can be parameterized on the basis of the observable physical structure of the landscape.

Work at LEO has focused on developing hillslope-scale closure relationships for discharge and for transport both by building on and testing existing theory, as well as by developing new approaches. Hillslope closure relations predicting discharge have been developed from the principles of hydraulic groundwater theory [86–88] and are being compared to both the

results of physical experiments and numerical models. Three-dimensional Richards equation-based models have been implemented to simulate flow and transport dynamics in the LEO hillslopes ([41, 49]; see also Section 2.1.7) and calibrated to reproduce the flow data with the physically justifiable parameter sets. **Figure 13** illustrates the observed storage-discharge relationship from one of the LEO hillslopes and a modeled relationship. The observed relationship shows a large degree of hysteresis, and the simulated relationship captures most of the features of this relationship. This type of hysteresis can be captured by the theoretical frameworks of Troch [88] and others, but not by the typical one-to-one storage-discharge relationships used in hydrologic models to simulate baseflow.

Projects at LEO have also driven the development of new parameterizations of hillslope-based transport that build on the concept of rank-storage selection functions (rSAS; [89]). This is a highly promising approach for a new generation of transport models [90]. rSAS theory depends on parameterization of probability distributions that capture the emergent effect of finer-scale processes determining transport through the hillslope. These functions extend the idea of a storage-discharge relationship: the function specifies not the overall discharge as a function of storage but rather the way the age distribution of discharge is selected from the age distribution of storage.

The PERTH (PERiodic Tracer Hierarchy) was developed to allow rSAS functions to be directly determined from the results of physical tracer experiments [14]. The key requirement is that the flow varies in a periodic way, so that the progressive breakthrough of a single tracer injection reveals information about the contribution to discharge of multiple ages at each time in the cycle. The LEO hillslope hydrodynamics can be controlled to allow precise observations of the flow and transport dynamics, and a large-scale PERTH-type experiment was conducted between 1 December 2016 and 28 December 2016. All three slopes were irrigated in

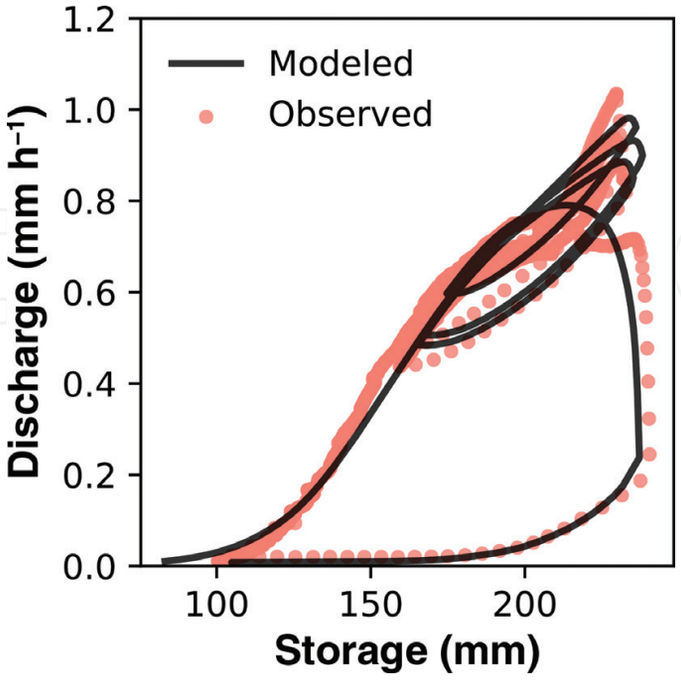

Figure 13. Observed and model storage-discharge relationship of a LEO landscape (for the period of 1–30 June 2015).

http://dx.doi.org/10.5772/intechopen.72325

an identical fashion every 3.5 days over the course of 4 weeks—a total of about 580 mm irrigations. The results are revealing much about the nature of hillslope rSAS functions.

These LEO experimental results can be extended to a wider class of idealized hillslopes through fine resolution modeling of system-scale flow and transport dynamics in "virtual hillslopes". The effect of variations in hillslope morphology, soil properties, and climate forcing on flow and transport closures can be examined using a three-dimensional Richards equation-based model and particle tracking algorithm validated against the LEO dataset. Moreover, the sensitivity of the parameterizations to observable physical properties (and their associated uncertainties) can be deduced.

However, LEO was inspired in part by efforts to go beyond the typical approach in hydrology of treating hydrologic properties as fixed features of the landscape, and instead ask deeper questions about why a landscape has the properties it does and how it came to be that way [91]. Physical, chemical, and biological data are also collected at LEO to connect the hydrologic behavior to interacting critical zone processes and ultimately to the coevolution of the system [3]. We aim to understand how the landscape internal structure evolves over time, feeding back on the flow and transport processes and modifying the emergent behavior that is the basis of flow and transport closure relations.

To develop improved predictive ability of the hydrological as well as biogeochemical and ecological responses in evolving landscapes, a second focus of the modeling at LEO is therefore the development of a coupled-process modeling framework. This modeling framework, referred to as TIMS (Section 2.1.7), aims to not only parameterize water flow and transport as functions of static landscape properties. Instead, it focuses specifically on coupling hydrological, microbial, geochemical, geomorphological, and ecological processes and considers the landscape properties themselves as dynamic. By attempting to predict dynamic landscape parameters based on a fundamental understanding of how they are created in the coevolution of a landscape, we may stand a chance to overcome the need for assumptions on unmeasurable "effective" model parameters and the inherent inability of most current modeling tools to represent integral adaptation to change (e.g., in climate).

At present, however, TIMS and other state-of-the-art Earth system models are still inadequate to represent many key Earth system processes that control long-term land-atmosphere exchanges of energy, water, and carbon. This is due to a lack of predictive understanding of the interactions between the relevant physical, chemical, and biological processes. Therefore, the modeling system will be continuously extended, synthesizing results from the physical experimentation at LEO to develop representations of critical process couplings that are currently not adequately represented. These include, for example, schemes to represent the evolution of landscape heterogeneity associated with transport and deposition of particles (colloids and sediments) and biogeochemical weathering, as well as associated feedbacks with the hydraulic properties of the LEO soils. Other areas of active model development include parameterizing leaf and root dynamics adaptive to environmental changes (e.g., high temperature and drought) and soil carbon dynamics as affected by geochemical reactions, microbial enzymes, climate, and water flow [33].

The observational and modeling results of experiments conducted under the present conditions will eventually be compared to results of identical experiments performed after the hillslopes

have been altered either through endogenous changes or through the introduction of new factors, such as the establishment of plants. As the LEO hillslopes evolve over time, we will iterate the physical and the numerical experiments to test hypotheses about the feedbacks between flow and transport dynamics and hillslope evolution. Lessons learned from failure and success in reproducing observations in the physical landscapes (see, e.g., [41]) will then be used to refine the mathematical representations and reduce uncertainties in model structures and parameters. The LEO landscapes and diverse modeling approaches are thereby anticipated to help fill the gap between plot-scale studies and larger scale (hillslope to global) model developments by constructing relationships between varying fluxes and states at the ZOB-scale, both through direct inference of closure relations and scaling of coupled-process modeling schemes. These developments may finally serve to project impacts of climate change on water resources as well as ecological processes and landscape evolution in varied environmental contexts.

3.2. Linking hydrological and geochemical processes in evolving landscapes

The nature of hydrological and geochemical interactions is a primary determinant of hillslope structure formation, available water quantity, and water quality along the entire evolutionary trajectory of a landscape—from pristine abiotic substrate subjected to a first rain pulse, when microbial (Section 3.3) and vascular plant (Section 3.4) life only begin to establish, to a matured landscape adjusting to variable climatic forcing. Examining and predicting the time evolution of subsurface structure through biogeochemical processes and its effect on hydrological partitioning and water residence time are therefore a key focus of the research at LEO. The LEO experiment provides unprecedented capability to examine the complex interactions that are integral to the hillslope evolution and soil formation processes because of the high density of hydrological and geochemical measurements in space and time, control of some of the drivers of weathering such as rainfall or temperature, and the ability to perform coupled hydrological-biogeochemical modeling.

In any developing landscape, including the LEO landscapes, the spatial structure of flow pathways along hillslopes determines the rate, extent, and distribution of geochemical reactions (and biological colonization) that drive weathering, the transport and precipitation of solutes and sediments, and the evolution of soil structure. The resulting structure and process evolution, in turn, induces spatiotemporal variability of hydrological states and flow pathways. Weathering reactions are strongly influenced by the time water spends along the subsurface flow paths [92, 93] at any stage of the landscape development. Dissolution of primary silicates is kinetically limited, and increasing residence time, and thus the duration of contact time of water with rocks, therefore potentially increases the concentration of lithogenic elements in the soil solution. The resulting relative saturation of soil solution (as measured by the saturation index) with respect to soil minerals will affect both primary mineral dissolution and secondary mineral precipitation [94]. The farther a solution is from equilibrium, the higher the rates of both dissolution and precipitation processes. In addition to water residence times, rock dissolution rates are also influenced by formation of secondary minerals [95]. Plants and microorganisms can also strongly influence weathering rates through production of organic acids and other complexing agents [72, 96], through respiration and uptake of water and dissolving nutrients [97], and through enzymatic promotion of bicarbonate formation from CO_2 [98, 99].

Since the distribution of microorganisms and vegetation on the slopes in space and time is driven by water and nutrient availability (Sections 3.3 and 3.4), biota will further complicate the already complex relationships between water flow and weathering in evolving hillslopes.

Precipitation of secondary minerals during incongruent weathering decreases the particle size of the soil, which affects its pore size distribution and hydraulic conductivity, and consequently the water transit times [100, 101]. Mineral precipitation can also feedback to further weathering [102, 103], nutrient and carbon retention, and microbial and plant distribution. Coupled geochemical-hydrological modeling (combined with pedotransfer functions) was performed for the LEO hillslopes to estimate mineral transformations and changes in soil hydraulic properties over a 10-year period with rainfall amount derived from several real-world locations in the southwestern United States [8]. The predictions suggested a significant increase in the fraction of secondary minerals and, as a result, a decrease in hydraulic conductivity over time. Predicted changes were highly variable in space, closely mirroring flow and saturation patterns on the hillslopes. It was further observed that solution-phase concentrations of lithogenic elements calculated by the models could provide early indication of the soil formation processes, even before changes in the solid phase would have become readily measurable. Since then, the physical experiments performed at LEO [54, 55] confirm both development of heterogeneity in the solution composition as a function of flow patterns and spatially resolved precipitation of secondary minerals as indicated by saturation indices for a number of minerals that would influence soil structure and flow patterns. For example, it can be seen for calcite (**Figure 14**) that there is pronounced spatial heterogeneity in the measurements linked to soil water content, and that there is a temporal progression in the saturation indices as the hillslope gets drier. Results from LEO soil cores further support spatially resolved precipitation of inorganic carbon through direct measurements (Section 2.5).

The geochemical evolution of a hillslope is also strongly linked to runoff generation. The fraction of incoming rainfall that eventually leaves the landscapes as seepage outflow (or overland flow, if any) affects the export of inorganic and organic compounds from the landscapes. This export process presents an integral part of soil formation. When soils age, their composition shifts toward elements such as iron and aluminum that form poorly soluble oxides and hydroxides, as these are retained. More soluble elements in turn are lost, such as silicon, which presents an originally predominant element on the landscape. Seepage generation additionally has significant implications for the carbon balance in the environment. The export of inorganic carbon that was previously captured in the landscape as a result of weathering (predominantly as bicarbonate and carbonate), and its transport and further storage in the oceans, serve as important mechanisms of carbon sequestration from the atmosphere. Weathering of basaltic rocks, such as those comprising the LEO landscapes, occurs rapidly [104], and our experiments showed that as much as 5 kg of carbon was lost from the hillslopes in a single rain event (see **Figure 8**; [54]). Finally, feedbacks between water flow, mineral weathering and soil formation, and biological activity can have important implications for water quality. These feedbacks control the off-site transport not only of lithogenic and biogenic compounds but also of potential anthropogenic and possibly hazardous compounds into streams and other downstream landscape elements.

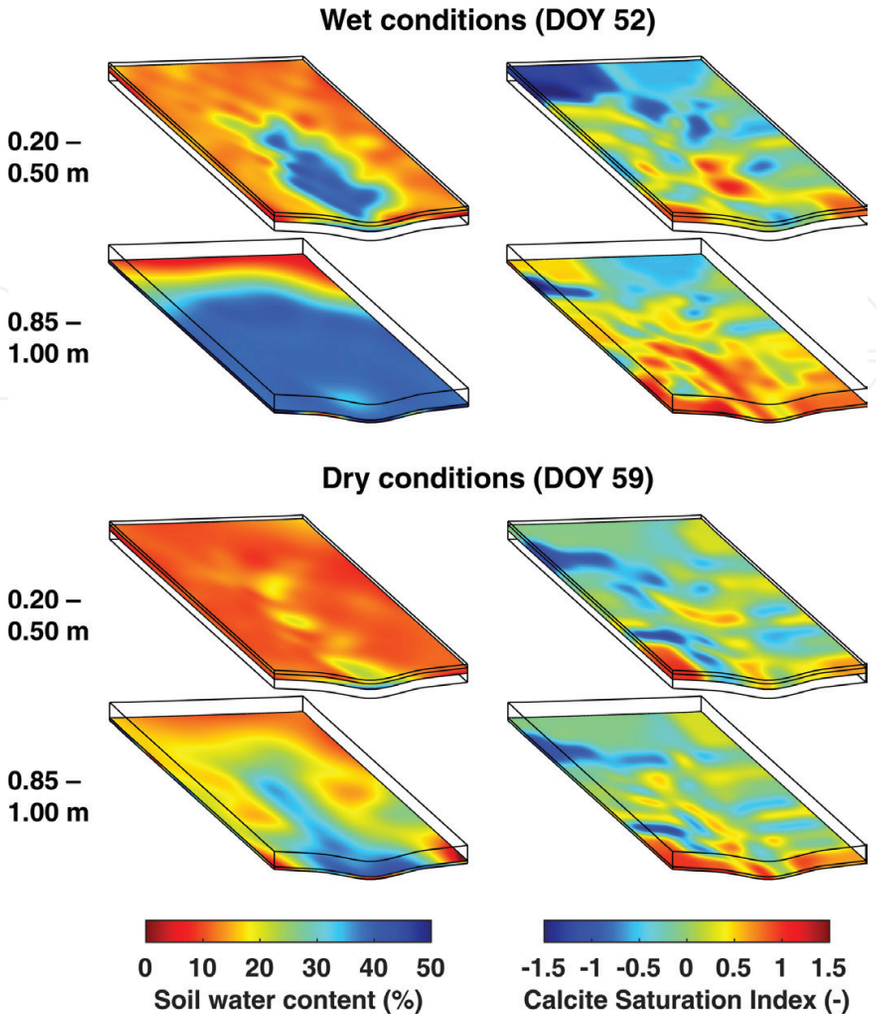

Figure 14. Three-dimensional interpolations of volumetric soil water content (SWC; left) and calcite saturation index (right) projected onto a LEO hillslope model at two depth intervals (0.20–0.50 m and 85–1.00 m) and two sampling dates (DOY 52 and DOY 59). For SWC: warm colors represent areas of relatively dry conditions while cool colors represent wet conditions. For calcite saturation index: warm colors represent areas of supersaturation while cool colors represent areas of reduced supersaturation or undersaturation. Note the unique scales for SWC (%) and saturation index (i.e., log Q/K).

3.3. Linking hydrological and microbial processes in evolving landscapes

Microorganisms typically represent the life pioneering initially abiotic, developing hillslopes. Microbial populations affect the trajectory and speed of evolution of physicochemical landscape properties and functions and may be critical in facilitating the establishment of vascular plant life (Section 3.4). Yet, we lack a clear picture of the manifold feedbacks between evolving patterns of microbial (and plant) ecology and physicochemical system dynamics across scales. In particular, our understanding of early-stage oligotrophic landscape elements is limited, as we rarely have the opportunity for their study in nature (but see related work by, e.g., [105, 106]) and typically lack the multifaceted observational density required. Microbial dynamics across incipient landscapes, such as the LEO hillslopes, are tightly linked to hydrological

and geochemical signatures. Hydrological flux processes themselves (e.g., infiltration, lateral redistribution of vadose zone water and groundwater, and evapotranspiration) and resulting soil moisture spatial and temporal dynamics are primarily controlled by structural properties of the subsurface and the driving forces of surface exchange. Hydrological dynamics, in turn, impact the time spent by a parcel of water in contact with microbial cells, the dissolution and flow of nutrients, and the movement of microbes in the system [107]. Additionally, hydrogeochemical processes, such as weathering and dissolution of primary minerals, dissolution of reactive phases, and reprecipitation of weathered elements, influence nutrient availability and may facilitate microbial colonization [108]. The concurrent microbial signatures of growth and function impact pore structure, weathering rate, and labile carbon deposition and thereby establish feedbacks of coupled hydro-biogeochemical processes influencing soil formation. Microbial life is therefore both a follower and facilitator of water flow paths in incipient landscape systems.

The heavily instrumented LEO landscapes, with the dense network of sensors and samplers and diverse modeling approaches, provide the opportunity to develop a mechanistic understanding of integrated hydrological and microbial processes occurring in the hillslopes as a result of their mutual interactions and to identify signatures that can be used to quantitatively characterize hydrology-microbiology relationships. For instance, it is important to understand how microbial cells and the biomolecules produced by the microbes are transported with the water. The time spent by a microbial community in a unique microenvironment impacts species-species interactions and accessibility of nutrients. Water movement also impacts the turnover of microbial community assemblies and has been shown to influence microbial ecological assembly processes [109]. However, many open questions remain regarding the nature of these interactions between hydrology and microbiology. Using **Figure 11** as an example, an unexpected trend was observed in the relative microbial abundances in the miniLEO small-scale model. While *Actinobacteria* were predominantly abundant at the surface, *Cyanobacteria* were found at greater depths in the model system. *Cyanobacteria* are photoautotrophs, i.e., they need sunlight to survive, and yet they occurred preferentially in deep and dark layers of the soil (highest abundance at 40 cm below the surface). In contrast, *Actinobacteria* were consistent in their localization toward the surface despite the potential for transport with water from the surface to deeper layers. Hypothesizing that water flow caused *Cyanobacteria* to travel deeper fails to explain why *Actinobacteria* maintained a constant relative abundance at the surface. So, are microbial species transported passively with the water depending on specific parameters such as cell size, or do they differ in their active movement (i.e., motility) and surface attachment (e.g., in biofilms)? Or are the relative abundance patterns simply imposed by the local environment and maintained by constant cell turnover rates, despite water flow? Tackling these questions requires combining hydrological tools with microbiological methods. For example, it will be relevant to incorporate microbial processes into reactive transport models and to evaluate average water volumes, transit times, and upstream flow path lengths associated with the microbial abundance patterns (e.g., for each voxel in the example **Figure 11**). Such distributed indices may facilitate the interfacing of hydrology and microbiology to study subsurface ecosystems.

3.4. Linking hydrological and plant ecological processes in evolving landscapes

The spatiotemporal interplay between water and vegetation dynamics, and their feedbacks to physicochemical landscape (Section 3.2) and microbial community (Section 3.3) organization, profoundly impacts the evolution of a hillslope and its cycling of mass and energy. Hydrological processes exert primary controls on the establishment, distribution, structure, and function of ecosystems, while biotic processes directly (e.g., through transpiration) and indirectly (e.g., through alteration of soil properties) affect the cycling of water through the landscape [110, 111]. A substantial body of ecohydrological research has examined plant-water interactions with respect to one-dimensional (vertical) water and nutrient fluxes at the patch scale [112], however, without incorporating lateral redistribution of water and nutrients imposed by hillslope morphology. Similarly, biogeography has been mindful of spatial patterns of drivers of vegetation distribution but has paid little attention to the inherent coevolution of the physical and biological realms as a process that drives the form and function of the biological and physical landscape. Due to their large scale and imposed gradients in topography and environmental conditions, as well as their climate control and monitoring capabilities, the LEO hillslopes provide the unique opportunity to tackle the gaps in our understanding of how physical-biological interactions drive landscape evolution in space and time. Working at the hillslope scale forces integration between one- and two-dimensional conceptualizations of ecohydrological processes and provides the topological structures that connect patches on the landscape by gravitational fluxes organized by hillslope morphology. From the patch or pedon perspective, the hillslope provides nonlocal controls on water and nutrient fluxes, while local controls at the patch scale influence downslope patches in the ecohydrological system.

The basic elements that define hillslope morphology, such as shape, gradient, aspect, and slope complexity (i.e., nonuniformity), affect water and energy availability (e.g., [3]). Hillslope shape expresses the convergence or divergence of surface flow paths in the planform (across slope) and profile (normal to slope) directions and therefore relates directly to soil moisture redistribution. Hillslope shape and gradient both affect runoff processes and erosion rates. Hillslope aspect directly influences irradiance and hence energy availability for evapotranspiration. Complex interactions at the hillslope scale between topography, soil development, runoff processes, and vegetation create self-reinforcing positive feedbacks in ecohydrological processes that must be considered to develop a comprehensive understanding of ecohydrological patterns and processes.

The effects of vegetation on physical processes will depend on the structure of the community [25]. One might hypothesize that shallow-rooted plants would have a much less significant impact on the ecohydrology of a hillslope than a deep-rooted shrub because they lack a physical integration with as much of the soil profile. But are ecohydrological process more influenced by percent cover of the soil (presumably higher in a lower-stature forb or grassland system), higher photosynthetic function that derives organic acids that can drive soil processes, or simply the water use efficiency of the vegetation, regardless of type? Aboveground-belowground linkages are so inherently complex that when we add discussion of connections among soil pedons in space or consider the various members of a vegetative community, how little we know about the ecohydrology at the hillslope scale becomes glaringly apparent.

http://dx.doi.org/10.5772/intechopen.72325

LEO is ideally suited to investigate the coevolution of water flow paths and plant ecological processes, soil properties, and microbial dynamics. After an initial period of bare soil conditions, seeds will be dispersed on the hillslope surfaces and vascular plant growth will strongly modify the surface and subsurface properties of the LEO landscapes. Differences in available water and nutrients in the subsurface, resulting from the coevolution of hydrological and biogeochemical processes prior to vegetation, will create niches that different plant species can occupy. These adaptation and selection mechanisms will result in whole-ecosystem dynamics that are different from a uniform distribution of plant species across the slopes. The aboveground and belowground instrumentation at LEO will allow the detailed monitoring of water, carbon, and energy fluxes at the land-atmosphere interface and throughout the hillslopes. Understanding these connections between the physical environment and germination and survival rates of various species will yield important information on characteristics of plant establishment. Following these patterns through time will allow for insights into those key processes of coevolution of plant-soil dynamics in the profile and planform.

4. Conclusions and outlook

This chapter has presented the research infrastructure, facilities, and initial experimental results of the Landscape Evolution Observatory (LEO) project at the Biosphere 2. LEO is a carefully designed and massively outfitted macrocosm experiment of an unprecedented scale and ambition of scope. Each of the three model landscapes emulates a pristine, sloping zero-order basin consisting of more than 500 metric tons of homogenous basaltic tephra housed within climate-controlled bays. The infrastructure operates dense arrays of more than 1900 sensors and samplers per landscape that are complemented by state-of-the-art research support systems, including an isotope and trace gas analysis network, electrical resistivity tomography instrumentation, high-resolution remote imaging systems, and advanced analytical capabilities for analyzing liquids and solids. The combined capacity of these structures allows tracking states, fluxes, and pathways of water, energy, and critical elements such as carbon at sub-meter to landscape scales, arguably representing the most successful attempt to closing hydro-biogeochemical budgets for a hillslope-size system to date. The system importantly allows key developmental processes to be rigorously tracked, including changes in subsurface and the development of microbial and ultimately vascular plant communities.

LEO is fully operational and has recently (October 2016) entered its 10-year long institutional experiment. During this experiment, variable climate forcing (mainly rainfall treatments) will drive the initially simple, abiotic model landscapes into life-sustaining ecosystems. After a first phase of bare soil surface conditions that is scheduled to last approximately 2 to 3 years, the landscapes will be colonized by vascular plants able to germinate and grow on the poorly developed LEO soil. While the landscapes evolve to increasingly complex states, Earth scientists will have the opportunity to iteratively build knowledge on the interactions

and feedbacks between hydrological, geochemical, geomorphological, microbial, and ecological processes that control landscape form and function, and to formalize this knowledge into distributed coupled-process models and closure relations at the hillslope-scale. The threefold replication of initial landscape conditions and climate treatment will thereby allow to develop and rigorously test (i.e., to accept or reject) laws of fundamental natural processes (e.g., flow and transport) at space-time scales relevant for prediction. In later phases, varying experimental treatments across the replicate slopes (e.g., different rainfall distribution, temperature or CO_2 levels) may drive divergent landscape evolutionary trajectories, which allow further evaluation and refinement of the knowledge and predictive capabilities gained.

The LEO infrastructure is designed as a community resource with open data availability and seeks to foster broad interdisciplinary collaboration and science planning. During the next 10 years, scientists from across the world will have the opportunity to propose smaller research projects that can be implemented without loss of objectives of the institutional experiment. For instance, researchers who would like to study certain rainfall-runoff dynamics can propose a sequence of rain events, or those commanding specific measurement or analysis capabilities are welcome to integrate those into existing efforts. Similarly, the reader is encouraged to contact the authors to share their ideas about research opportunities with respect to the planned evolutionary forcing of the landscapes. For example, the composition of the seed pool for the upcoming vascular plant colonization is still under debate. By rapidly iterating dense experimental measurement with community-based planning, data analysis, and model development, we envision that our understanding and ability to predict the coevolution of hydrological, biogeochemical, and ecological processes and their interactions under variable climate can be significantly improved. This vision will be tested when we ultimately extrapolate our understanding of abiotic-biotic system coevolution into the complex reality of natural environments to meet the challenge of predicting landscape-scale response to global change.

Acknowledgements

The authors gratefully acknowledge support from the Philecology Foundation of Fort Worth Texas, the National Science Foundation (NSF; NSF-funded project 1344552, NSF-funded Hydrologic Synthesis Project: Water cycle dynamics in a changing environment: advancing hydrologic science through synthesis, NSF grant EAR-0636043, NSF grant EAR-1340912, NSF grant EAR-1417097), and the Department of Energy (Joint Genome Institute small scale Community Science Program grant 502880). Additional funding support was provided by the Office of the Vice President of Research at the University of Arizona and by the Technology and Research Initiative Fund (TRIF) Water, Environmental, and Energy Solutions (WEES) initiative at the University of Arizona (Shared Equipment Enhancement Funds). PT is grateful for financial support from the Agnese Nelms Haury Program.

http://dx.doi.org/10.5772/intechopen.72325

Author details

Till H. M. Volkmann[1]*, Aditi Sengupta[1], Luke A. Pangle[2], Katerina Dontsova[1], Greg A. Barron-Gafford[3], Ciaran J. Harman[4], Guo-Yue Niu[5], Laura K. Meredith[6], Nate Abramson[1], Antonio A. Meira Neto[5], Yadi Wang[7], John R. Adams[1], David D. Breshears[6,8], Aaron Bugaj[1], Jon Chorover[6,7], Alejandro Cueva[1], Stephen B. DeLong[9], Matej Durcik[5], Ty P. A. Ferre[5], Edward A. Hunt[1], Travis E. Huxman[10], Minseok Kim[4], Raina M. Maier[7], Russell K. Monson[6], Jon D. Pelletier[11], Michael Pohlmann[7], Craig Rasmussen[7], Joaquin Ruiz[1,11], Scott R. Saleska[8], Marcel G. Schaap[7], Michael Sibayan[1], Markus Tuller[7], Joost L. M. van Haren[1], Xubin Zeng[5] and Peter A. Troch[1,5]

*Address all correspondence to: tillv@email.arizona.edu

1 University of Arizona, Biosphere 2, Tucson, AZ, USA

2 Georgia State University, Department of Geosciences, Atlanta, GA, USA

3 University of Arizona, School of Geography and Development, Tucson, AZ, USA

4 Johns Hopkins University, Department of Geography and Environmental Engineering, Baltimore, MD, USA

5 University of Arizona, Department of Hydrology and Atmospheric Sciences, Tucson, AZ, USA

6 University of Arizona, School of Natural Resources and the Environment, Tucson, AZ, USA

7 University of Arizona, Department of Soil, Water and Environmental Science, Tucson, AZ, USA

8 University of Arizona, Department of Ecology and Evolutionary Biology, Tucson, AZ, USA

9 United States Geological Survey, Menlo Park, CA, USA

10 University of California at Irvine, Center for Environmental Biology, Irvine, CA, USA

11 University of Arizona, Department of Geosciences, Tucson, AZ, USA

References

[1] Troch PA, Carrillo GA, Heidbüchel I, Rajagopal S, Switanek M, Volkmann THM, et al. Dealing with landscape heterogeneity in watershed hydrology: A review of recent progress toward new hydrological theory. Geography Compass. 2009;**3**(1):375-392

[2] Troch PA, Lahmers T, Meira A, Mukherjee R, Pedersen JW, Roy T, et al. Catchment coevolution: A useful framework for improving predictions of hydrological change? Water Resources Research. 2015;**51**(7):4903-4922

[3] Pelletier JD, Barron-Gafford GA, Breshears DD, Brooks PD, Chorover J, Durcik M, et al. Coevolution of nonlinear trends in vegetation, soils, and topography with elevation and slope aspect: A case study in the sky islands of southern Arizona. Journal of Geophysical Research - Earth Surface. 2013;**118**(2):741-758

[4] Brantley S, White TS, White AF, Sparks D, Richter D, Pregitzer K, et al. Frontiers in Exploration of the Critical Zone: Report of a NSF-Sponsored Workshop. VA, USA: Arlington; 2006:**30**

[5] Chorover J, Troch PA, Rasmussen C, Brooks PD, Pelletier JD, Breshears DD, et al. How water, carbon, and energy drive critical zone evolution: The Jemez–Santa Catalina critical zone observatory. Vadose Zone Journal. 2011;**10**(3):884-899

[6] Ivanov VY, Fatichi S, Jenerette GD, Espeleta JF, Troch PA, Huxman TE. Hysteresis of soil moisture spatial heterogeneity and the "homogenizing" effect of vegetation. Water Resources Research. 2010;**46**(9):W09521

[7] Hopp L, Harman C, Desilets SLE, Graham CB, McDonnell JJ, Troch PA. Hillslope hydrology under glass: Confronting fundamental questions of soil-water-biota co-evolution at Biosphere 2. Hydrology and Earth System Sciences. 2009;**13**(11):2105-2118

[8] Dontsova K, Steefel CI, Desilets S, Thompson A, Chorover J. Solid phase evolution in the Biosphere 2 hillslope experiment as predicted by modeling of hydrologic and geochemical fluxes. Hydrology and Earth System Sciences. 2009;**13**(12):2273-2286

[9] White T, Brantley S, Banwart S, Chorover J, Dietrich W, Derry L, et al. The role of critical zone observatories in critical zone science. In: Giardino R, Hauser C, editors. Principles and Dynamics of the Critical Zone. Amsterdam, Netherlands: Elsevier; 2015. pp. 15-78

[10] Pangle LA, DeLong SB, Abramson N, Adams J, Barron-Gafford GA, Breshears DD, et al. The Landscape Evolution Observatory: A large-scale controllable infrastructure to study coupled earth-surface processes. Geomorphology. 2015;**244**:190-203

[11] Dietrich WE, Reneau SL, Wilson CJ. Overview: Zero-order basins and problems of drainage density, sediment transport and hillslope morphology. International Association of Scientific Hydrology. 1987;**165**:27-37

[12] Finn M. The mangrove mesocosm of Biosphere 2: Design, establishment and preliminary results. Ecological Engineering. 1996;**6**(1):21-56

[13] Marino BDV, Mahato TR, Druitt JW, Leigh L, Lin G, Russell RM, et al. The agricultural biome of Biosphere 2: Structure, composition and function. Ecological Engineering. 1999;**13**(1):199-234

[14] Kim M, Pangle LA, Cardoso C, Lora M, Volkmann THM, Wang Y, et al. Transit time distributions and StorAge selection functions in a sloping soil lysimeter with time-varying flow paths: Direct observation of internal and external transport variability. Water Resources Research. 2016;**52**(9):7105-7129

[15] Pangle LA, Kim M, Cardoso C, Lora M, Meira Neto AA, Volkmann THM, et al. The mechanistic basis for storage-dependent age distributions of water discharged from an experimental hillslope. Water Resources Research. 2017;**53**(4):2733-2754

[16] Los Gatos Research Inc. Isotopic Water Analyzer (δ^2H, $\delta^{17}O$, $\delta^{18}O$) - Enhanced Performance. 2015. Available from: www.lgrinc.com/documents/LGR_IWA-45EP.pdf

[17] McManus JB, Nelson DD, Zahniser MS. Design and performance of a dual-laser instrument for multiple isotopologues of carbon dioxide and water. Optics Express. 2015;**23**(5):6569-6586

[18] Nelson DD, McManus JB, Herndon SC, Zahniser MS, Tuzson B, Emmenegger L. New method for isotopic ratio measurements of atmospheric carbon dioxide using a 4.3 μm pulsed quantum cascade laser. Applied Physics B. 2008;**90**(2):301-309

[19] Tuzson B, Mohn J, Zeeman MJ, Werner RA, Eugster W, Zahniser MS, et al. High precision and continuous field measurements of $\delta^{13}C$ and $\delta^{18}O$ in carbon dioxide with a cryogen-free QCLAS. Applied Physics B. 2008;**92**(3):451-458

[20] Baer DS, Paul JB, Gupta JB, O'Keefe A. Sensitive absorption measurements in the near-infrared region using off-axis integrated-cavity-output spectroscopy. Applied Physics B: Lasers and Optics. 2002;**75**(2-3):261-265

[21] McManus JB, Zahniser MS, Nelson DD, Shorter JH, Herndon SC, Jervis D, et al. Recent progress in laser-based trace gas instruments: Performance and noise analysis. Applied Physics B. 2015;**119**(1):203-218

[22] Pangle LA, Klaus J, Berman ESF, Gupta M, McDonnell JJ. A new multisource and high-frequency approach to measuring δ^2H and $\delta^{18}O$ in hydrological field studies. Water Resources Research. 2013;**49**(11):7797-7803

[23] Mathieu R, Bariac T. A numerical model for the simulation of stable isotope profiles in drying soils. Journal of Geophysical Research. 1996;**101**(D7):12685-12696

[24] Volkmann THM, Weiler M. Continual in situ monitoring of pore water stable isotopes in the subsurface. Hydrology and Earth System Sciences. 2014;**18**(5):1819-1833

[25] Volkmann THM, Haberer K, Gessler A, Weiler M. High-resolution isotope measurements resolve rapid ecohydrological dynamics at the soil–plant interface. The New Phytologist. 2016;**210**(3):839-849

[26] Volkmann THM, Kühnhammer K, Herbstritt B, Gessler A, Weiler M. A method for in situ monitoring of the isotope composition of tree xylem water using laser spectroscopy. Plant, Cell and Environment. 2016;**39**(9):2055-2063

[27] Shahraeeni E, Or D. Thermo-evaporative fluxes from heterogeneous porous surfaces resolved by infrared thermography. Water Resources Research. 2010;**46**(9):W09511

[28] Vereecken H, Huisman JA, Pachepsky Y, Montzka C, van der Kruk J, Bogena H, et al. On the spatio-temporal dynamics of soil moisture at the field scale. Journal of Hydrology. 2014;**516**:76-96

[29] Samouëlian A, Cousin I, Tabbagh A, Bruand A, Richard G. Electrical resistivity survey in soil science: A review. Soil and Tillage Research. 2005;**83**(2):173-193

[30] Niu G-Y, Paniconi C, Troch PA, Scott RL, Durcik M, Zeng X, et al. An integrated modelling framework of catchment-scale ecohydrological processes: 1. Model description and tests over an energy-limited watershed. Ecohydrology. 2014;**7**(2):427-439

[31] Niu G-Y, Troch PA, Paniconi C, Scott RL, Durcik M, Zeng X, et al. An integrated modelling framework of catchment-scale ecohydrological processes: 2. The role of water subsidy by overland flow on vegetation dynamics in a semi-arid catchment. Ecohydrology. 2014;**7**(2):815-827

[32] Fang Y-H, Zhang X, Niu G-Y, Zeng W, Zhu J, Zhang T. Study of the spatiotemporal characteristics of meltwater contribution to the total runoff in the upper Changjiang River basin. Water. 2017;**9**(3):165

[33] Zhang X, Niu G-Y, Elshall AS, Ye M, Barron-Gafford GA, Pavao-Zuckerman M. Assessing five evolving microbial enzyme models against field measurements from a semiarid savannah—What are the mechanisms of soil respiration pulses? Geophysical Research Letters. 2014;**41**(18):6428-6434

[34] Camporese M, Paniconi C, Putti M, Orlandini S. Surface-subsurface flow modeling with path-based runoff routing, boundary condition-based coupling, and assimilation of multisource observation data. Water Resources Research. 2010;**46**(2):W02512

[35] Paniconi C, Putti M. A comparison of Picard and Newton iteration in the numerical solution of multidimensional variably saturated flow problems. Water Resources Research. 1994;**30**(12):3357-3374

[36] Orlandini S, Rosso R. Parameterization of stream channel geometry in the distributed modeling of catchment dynamics. Water Resources Research. 1998;**34**(8):1971-1985

[37] Niu G-Y, Yang Z-L, Mitchell KE, Chen F, Ek MB, Barlage M, et al. The community Noah land surface model with multiparameterization options (Noah-MP): 1. Model description and evaluation with local-scale measurements. Journal of Geophysical Research, [Atmospheres]. 2011;**116**(D12):D12109

[38] Peters DPC. Plant species dominance at a grassland–shrubland ecotone: An individual-based gap dynamics model of herbaceous and woody species. Ecological Modelling. 2002;**152**(1):5-32

[39] Steefel C. GIMRT, Version 1.2: Software for Modeling Multicomponent, Multidimensional Reactive Transport. User's Guide, UCRL-MA-143182. Lawrence Livermore National Laboratory: Livermore, CA, USA; 2001

[40] Sivapalan M. Pattern, process and function: Elements of a unified theory of hydrology at the catchment scale. In: Anderson MG, editor. Encyclopedia of Hydrological Sciences. Chichester, England: Wiley; 2005. pp. 193-219

[41] Niu GY, Pasetto D, Scudeler C, Paniconi C, Putti M, Troch PA, et al. Incipient subsurface heterogeneity and its effect on overland flow generation – Insight from a modeling study of the first experiment at the Biosphere 2 Landscape Evolution Observatory. Hydrology and Earth System Sciences. 2014;**18**(5):1873-1883

[42] Nijland W, van der Meijde M, Addink EA, de Jong SM. Detection of soil moisture and vegetation water abstraction in a Mediterranean natural area using electrical resistivity tomography. Catena. 2010;**81**(3):209-216

[43] Ferré T, Bentley L, Binley A, Linde N, Kemna A, Singha K, et al. Critical steps for the continuing advancement of hydrogeophysics. Eos, Transactions American Geophysical Union. 2009;**90**(23):200-200

[44] Baldocchi D, Falge E, Gu LH, Olson R, Hollinger D, Running S, et al. FLUXNET: A new tool to study the temporal and spatial variability of ecosystem-scale carbon dioxide, water vapor, and energy flux densities. Bulletin of the American Meteorological Society. 2001;**82**(11):2415-2434

[45] Meredith LK, Commane R, Munger JW, Dunn A, Tang J, Wofsy SC, et al. Ecosystem fluxes of hydrogen: A comparison of flux-gradient methods. Atmospheric Measurement Techniques. 2014;**7**(9):2787-2805

[46] Altaf Arain M, James Shuttleworth W, Farnsworth B, Adams J, Lutfi SO. Comparing micrometeorology of rain forests in Biosphere-2 and Amazon basin. Agricultural and Forest Meteorology. 2000;**100**(4):273-289

[47] Zeng X, Wang Z, Wang A. Surface skin temperature and the interplay between sensible and ground heat fluxes over arid regions. Journal of Hydrometeorology. 2012; **13**(4):1359-1370

[48] Sprenger M, Volkmann THM, Blume T, Weiler M. Estimating flow and transport parameters in the unsaturated zone with pore water stable isotopes. Hydrology and Earth System Sciences. 2015;**19**(6):2617-2635

[49] Scudeler C, Pangle LA, Pasetto D, Niu GY, Volkmann THM, Paniconi C, et al. Multiresponse modeling of variably saturated flow and isotope tracer transport for a hillslope experiment at the Landscape Evolution Observatory. Hydrology and Earth System Sciences. 2016;**20**(10):4061-4078

[50] Reichstein M, Falge E, Baldocchi D, Papale D, Aubinet M, Berbigier P, et al. On the separation of net ecosystem exchange into assimilation and ecosystem respiration: Review and improved algorithm. Global Change Biology. 2005;**11**(9):1424-1439

[51] Phillips CL, Gregg JW, Wilson JK. Reduced diurnal temperature range does not change warming impacts on ecosystem carbon balance of Mediterranean grassland mesocosms. Global Change Biology. 2011;**17**(11):3263-3273

[52] Bowling DR, Pataki DE, Randerson JT. Carbon isotopes in terrestrial ecosystem pools and CO_2 fluxes. The New Phytologist. 2008;**178**(1):24-40

[53] Berry J, Wolf A, Campbell JE, Baker I, Blake N, Blake D, et al. A coupled model of the global cycles of carbonyl sulfide and CO_2: A possible new window on the carbon cycle. Journal of Geophysical Research – Biogeosciences. 2013;**118**(2):842-852

[54] van Haren J, Dontsova K, Barron-Gafford GA, Troch PA, Chorover J, Delong SB, et al. CO_2 diffusion into pore spaces limits weathering rate of an experimental basalt landscape. Geology. 2017;**45**(3):203-206

[55] Pohlmann M, Dontsova K, Root R, Ruiz J, Troch P, Chorover J. Pore water chemistry reveals gradients in mineral transformation across a model basaltic hillslope. Geochemistry, Geophysics, Geosystems. 2016;**17**(6):2054-2069

[56] Sengupta A, Stegen JC, Nielson JW, Meira-Neto A, Wang Y, Troch PA, et al. Assessment of microbial community patterns under incipient conditions in a basalt soil system. Manuscript in preparation

[57] Barron-Gafford GA, Sanchez-Cañete EP, Minor RL, Hendryx SM, Lee E, Sutter LF, et al. Impacts of hydraulic redistribution on grass–tree competition vs facilitation in a semi-arid savanna. The New Phytologist. 2017;**215**(4):1451-1461

[58] Potts DL, Minor RL, Braun Z, Barron-Gafford GA. Photosynthetic phenological variation may promote coexistence among co-dominant tree species in a Madrean sky island mixed conifer forest. Tree Physiology. 2017;**37**(9):1229-1238

[59] Ustin SL, Roberts DA, Gamon JA, Asner GP, Green RO. Using imaging spectroscopy to study ecosystem processes and properties. Bioscience. 2004;**54**(6):523-534

[60] Beer C, Reichstein M, Tomelleri E, Ciais P, Jung M, Carvalhais N, et al. Terrestrial gross carbon dioxide uptake: Global distribution and covariation with climate. Science. 2010;**329**(5993):834-838

[61] Zhao M, Running SW. Drought-induced reduction in global terrestrial net primary production from 2000 through 2009. Science. 2010;**329**(5994):940-943

[62] Zhao M, Heinsch FA, Nemani RR, Running SW. Improvements of the MODIS terrestrial gross and net primary production global data set. Remote Sensing of Environment. 2005;**95**(2):164-176

[63] Friedlingstein P, Cox P, Betts R, Bopp L, Bloh WV, Brovkin V, et al. Climate–carbon cycle feedback analysis: Results from the C4MIP model intercomparison. Journal of Climate. 2006;**19**(14):3337-3353

[64] Damm A, Elbers JAN, Erler A, Gioli B, Hamdi K, Hutjes R, et al. Remote sensing of sun-induced fluorescence to improve modeling of diurnal courses of gross primary production (GPP). Global Change Biology. 2010;**16**(1):171-186

[65] Frankenberg C, Fisher JB, Worden J, Badgley G, Saatchi SS, Lee J-E, et al. New global observations of the terrestrial carbon cycle from GOSAT: Patterns of plant fluorescence with gross primary productivity. Geophysical Research Letters. 2011;**38**(17):L17706

[66] Rascher U, Agati G, Alonso L, Cecchi G, Champagne S, Colombo R, et al. CEFLES2: The remote sensing component to quantify photosynthetic efficiency from the leaf to the region by measuring sun-induced fluorescence in the oxygen absorption bands. Biogeosciences. 2009;**6**(7):1181-1198

[67] Zarco-Tejada PJ, González-Dugo V, Berni JAJ. Fluorescence, temperature and narrow-band indices acquired from a UAV platform for water stress detection using a micro-hyperspectral imager and a thermal camera. Remote Sensing of Environment. 2012;**117**:322-337

[68] Amoros-Lopez J, Gomez-Chova L, Vila-Frances J, Alonso L, Calpe J, Moreno J, et al. Evaluation of remote sensing of vegetation fluorescence by the analysis of diurnal cycles. International Journal of Remote Sensing. 2008;**29**(17-18):5423-5436

[69] Stumm W, Morgan JJ. Aquatic Chemistry: Chemical Equilibria and Rates in Natural Waters. 3rd ed. Chichester, England: Wiley; 1996

[70] Torn MS, Trumbore SE, Chadwick OA, Vitousek PM, Hendricks DM. Mineral control of soil organic carbon storage and turnover. Nature. 1997;**389**(6647):170-173

[71] Chorover J, Amistadi MK, Chadwick OA. Surface charge evolution of mineral-organic complexes during pedogenesis in Hawaiian basalt. Geochimica et Cosmochimica Acta. 2004;**68**(23):4859-4876

[72] Dontsova K, Zaharescu D, Henderson W, Verghese S, Perdrial N, Hunt E, et al. Impact of organic carbon on weathering and chemical denudation of granular basalt. Geochimica et Cosmochimica Acta. 2014;**139**:508-526

[73] Jencso KG, McGlynn BL. Hierarchical controls on runoff generation: Topographically driven hydrologic connectivity, geology, and vegetation. Water Resources Research. 2011; **47**(11):W11527

[74] Nippgen F, McGlynn BL, Marshall LA, Emanuel RE. Landscape structure and climate influences on hydrologic response. Water Resources Research. 2011;**47**(12):W12528

[75] Buttle JM, Dillon PJ, Eerkes GR. Hydrologic coupling of slopes, riparian zones and streams: An example from the Canadian shield. Journal of Hydrology. 2004;**287**(1):161-177

[76] Detty JM, McGuire KJ. Topographic controls on shallow groundwater dynamics: Implications of hydrologic connectivity between hillslopes and riparian zones in a till mantled catchment. Hydrological Processes. 2010;**24**(16):2222-2236

[77] Bencala KE, Gooseff MN, Kimball BA. Rethinking hyporheic flow and transient storage to advance understanding of stream-catchment connections. Water Resources Research. 2011;**47**(3):W00H3

[78] Beven K. Searching for the holy grail of scientific hydrology: $Q_t=(S, R, \Delta t)A$ as closure. Hydrology and Earth System Sciences. 2006;**10**(5):609-618

[79] Kirchner JW. Getting the right answers for the right reasons: Linking measurements, analyses, and models to advance the science of hydrology. Water Resources Research. 2006;**42**(3):W03S4

[80] McDonnell JJ, Sivapalan M, Vaché K, Dunn S, Grant G, Haggerty R, et al. Moving beyond heterogeneity and process complexity: A new vision for watershed hydrology. Water Resources Research. 2007;**43**(7):W07301

[81] Reggiani P, Sivapalan M, Hassanizadeh SM. A unifying framework of watershed thermodynamics: Balance equations for mass, momentum, energy and entropy and the second law of thermodynamics. Advances in Water Resources. 1998;**22**(4):367-398

[82] Reggiani P, Sivapalan M, Hassanizadeh SM. Conservation equations governing hillslope responses: Exploring the physical basis of water balance. Water Resources Research. 2000;**36**(7):1845-1863

[83] Reggiani P, Sivapalan M, Hassanizadeh SM, Gray WG. Coupled equations for mass and momentum balance in a stream network: Theoretical derivation and computational experiments. Proceedings of the Royal Society London, A. 2001;**457**(2005):157-189

[84] Kirchner JW. Catchments as simple dynamical systems: Catchment characterization, rainfall-runoff modeling, and doing hydrology backward. Water Resources Research. 2009;**45**(2):W02429

[85] Wittenberg H. Baseflow recession and recharge as nonlinear storage processes. Hydrological Processes. 1999;**13**(5):715-726

[86] Brutsaert W. The unit response of groundwater outflow from a hillslope. Water Resources Research. 1994;**30**(10):2759-2763

[87] Harman CJ, Reeves DM, Baeumer B, Sivapalan M. A subordinated kinematic wave equation for heavy-tailed flow responses from heterogeneous hillslopes. Journal of Geophysical Research - Earth Surface. 2010;**115**(F1):F00A8

[88] Troch PA, Paniconi C, Emiel van Loon E. Hillslope-storage Boussinesq model for subsurface flow and variable source areas along complex hillslopes: 1. Formulation and characteristic response. Water Resources Research. 2003;**39**(11):1316

[89] Harman CJ. Time-variable transit time distributions and transport: Theory and application to storage-dependent transport of chloride in a watershed. Water Resources Research. 2015;**51**(1):1-30

[90] Rinaldo A, Benettin P, Harman CJ, Hrachowitz M, McGuire KJ, van der Velde Y, et al. Storage selection functions: A coherent framework for quantifying how catchments store and release water and solutes. Water Resources Research. 2015;**51**(6):4840-4847

[91] Harman C, Troch PA. What makes Darwinian hydrology "Darwinian"? Asking a different kind of question about landscapes. Hydrology and Earth System Sciences. 2014;**18**(2):417-433

[92] Steefel CI. Geochemical kinetics and transport. In: Brantley SL, Kubicki JD, White AF, editors. Kinetics of Water-Rock Interaction. NY, USA: Springer; 2008. pp. 545-589

[93] Maher K. The role of fluid residence time and topographic scales in determining chemical fluxes from landscapes. Earth and Planetary Science Letters. 2011;**312**(1):48-58

[94] Maher K, Steefel CI, White AF, Stonestrom DA. The role of reaction affinity and secondary minerals in regulating chemical weathering rates at the Santa Cruz soil Chronosequence, California. Geochim Cosmochim Acta. 2009;**73**(10):2804-2831

[95] Yokoyama T, Banfield JF. Direct determinations of the rates of rhyolite dissolution and clay formation over 52,000 years and comparison with laboratory measurements. Geochimica et Cosmochimica Acta. 2002;**66**(15):2665-2681

[96] Neaman A, Chorover J, Brantley SL. Implications of the evolution of organic acid moieties for basalt weathering over geological time. American Journal of Science. 2005; **305**(2):147-185

[97] Zaharescu DG, Burghelea CI, Dontsova K, Presler JK, Maier RM, Huxman T, et al. Ecosystem composition controls the early fate of rare earth elements during incipient soil genesis. BioRxiv. 2016;061846

[98] Lian B, Xiao L, Sun Q. Ecological effects of the microbial weathering of silicate minerals. Acta Geologica Sinica - English Edition. 2017;**91**(s1):150-152

[99] Xiao L, Lian B, Hao J, Liu C, Wang S. Effect of carbonic anhydrase on silicate weathering and carbonate formation at present day CO_2 concentrations compared to primordial values. Scientific Reports. 2015;**5**:7733

[100] Li L, Steefel CI, Yang L. Scale dependence of mineral dissolution rates within single pores and fractures. Geochimica et Cosmochimica Acta. 2008;**72**(2):360-377

[101] Pacheco FAL, Van der Weijden CH. Integrating topography, hydrology and rock structure in weathering rate models of spring watersheds. Journal of Hydrology. 2012; **428**:32-50

[102] Anbeek C. The effect of natural weathering on dissolution rates. Geochimica et Cosmochimica Acta. 1993;**57**(21):4963-4975

[103] Brantley SL, Mellott NP. Surface area and porosity of primary silicate minerals. American Mineralogist. 2000;**85**(11-12):1767-1783

[104] Gislason SR, Oelkers EH, Eiriksdottir ES, Kardjilov MI, Gisladottir G, Sigfusson B, et al. The feedback between climate and weathering. Mineralogical Magazine. 2008; **72**(1):317-320

[105] Valentín-Vargas A, Root RA, Neilson JW, Chorover J, Maier RM. Environmental factors influencing the structural dynamics of soil microbial communities during assisted phytostabilization of acid-generating mine tailings: A mesocosm experiment. Science of the Total Environment. 2014;**500**:314-324

[106] Neilson JW, Quade J, Ortiz M, Nelson WM, Legatzki A, Tian F, et al. Life at the hyperarid margin: Novel bacterial diversity in arid soils of the Atacama Desert, Chile. Extremophiles. 2012;**16**(3):553-566

[107] Wang Y, Bradford SA, Šimůnek J. Transport and fate of microorganisms in soils with preferential flow under different solution chemistry conditions. Water Resources Research. 2013;**49**(5):2424-2436

[108] Banfield JF, Barker WW, Welch SA, Taunton A. Biological impact on mineral dissolution: Application of the lichen model to understanding mineral weathering in the rhizosphere. Proceedings of the National Academy of Sciences. 1999;**96**(7):3404-3411

[109] Graham EB, Crump AR, Resch CT, Fansler S, Arntzen E, Kennedy DW, et al. Coupling spatiotemporal community assembly processes to changes in microbial metabolism. Frontiers in Microbiology. 2016;**7**:1949

[110] Angers DA, Caron J. Plant-induced changes in soil structure: Processes and feedbacks. Biogeochemistry. 1998;**42**(1-2):55-72

[111] Porporato A, Daly E, Rodriguez-Iturbe I. Soil water balance and ecosystem response to climate change. The American Naturalist. 2004;**164**(5):625-632

[112] Asbjornsen H, Goldsmith GR, Alvarado-Barrientos MS, Rebel K, Van Osch FP, Rietkerk M, et al. Ecohydrological advances and applications in plant–water relations research: A review. Journal of Plant Ecology. 2011;**4**(1-2):3-22

IntechOpen